Title

SPRY4-dependent ERK negative feedback demarcates functional adult stem cells in the male mouse germline†.

Journal

Biology of Reproduction, 109(4)

Authors

Luo, Yanyun
Yamada, Makiko
NTumba-Byn, Thierry
et al.

Publication Date

2023-10-13

DOI

10.1093/biolre/ioad089

Biology of Reproduction, 2023, **109(4)**, 533–551
https://doi.org/10.1093/biolre/ioad089
Advance access publication date 8 August 2023
Research Article

SPRY4-dependent ERK negative feedback demarcates functional adult stem cells in the male mouse germline†

Yanyun Luo[1], Makiko Yamada[1], Thierry N'Tumba-Byn[1], Hana Asif[1], Meng Gao[1], Yang Hu[2], Pauline Marangoni[3,4], Ying Liu[5], Todd Evans[1], Shahin Rafii[5], Ophir D. Klein[3,4], Henning U. Voss[6], Anna-Katerina Hadjantonakis[7], Olivier Elemento[2,8], Laura A. Martin[9,*] and Marco Seandel[1,*]

[1]Department of Surgery, Weill Cornell Medicine, New York, NY, USA
[2]Department of Physiology and Biophysics, Weill Cornell Medicine, New York, NY, USA
[3]Program in Craniofacial Biology, Department of Orofacial Sciences, University of California, San Francisco, CA, USA
[4]Department of Pediatrics and Institute for Human Genetics, University of California, San Francisco, CA, USA
[5]Division of Regenerative Medicine, Department of Medicine, Hartman Institute for Therapeutic Organ Regeneration, Ansary Stem Cell Institute, Weill Cornell Medicine, New York, NY, USA
[6]College of Human Ecology, Cornell University, Ithaca, NY, USA
[7]Developmental Biology Program, Sloan Kettering Institute, Memorial Sloan Kettering Cancer Center, New York, NY, USA
[8]Department of Physiology and Biophysics, Caryl and Israel Englander Institute for Precision Medicine, Weill Cornell Medicine, New York, NY, USA
[9]The New York Stem Cell Foundation Research Institute, New York, NY, USA

***Correspondence:** Department of Surgery, Weill Cornell Medicine, 1300 York Ave, Box 282, New York, NY 10065, USA. Tel: +12127463071; Fax: +12127468572; E-mail: mas9066@med.cornell.edu; New York Stem Cell Foundation, 619 West 54th Street, 3rd Floor, New York, NY 10019, USA. Tel: +16462137784; Fax: +12127875844; E-mail: landresmartin@NYSCF.org

†**Grant Support:** This work was supported in part as follows: R01 HD101452 from the National Institute of Child Health and Human Development, the Irma T. Hirschl and Monique Weill-Caulier Charitable Trusts, Gladys and Roland Harriman Foundation, and by the Bohmfalk Charitable Trust Fund (MS); by a New York Stem Cell Foundation–Druckenmiller Fellow Award (LM); by a Tri-Institutional Starr Stem Cell Scholars Fellowship (MY); and by a fellowship from the New York State Department of Health (NYSTEM training program) contract C32558GG (YL).

Abstract

Niche-derived growth factors support self-renewal of mouse spermatogonial stem and progenitor cells through ERK MAPK signaling and other pathways. At the same time, dysregulated growth factor-dependent signaling has been associated with loss of stem cell activity and aberrant differentiation. We hypothesized that growth factor signaling through the ERK MAPK pathway in spermatogonial stem cells is tightly regulated within a narrow range through distinct intracellular negative feedback regulators. Evaluation of candidate extracellular signal-regulated kinase (ERK) mitogen-activated protein kinase (MAPK)-responsive genes known to dampen downstream signaling revealed robust induction of specific negative feedback regulators, including *Spry4*, in cultured mouse spermatogonial stem cells in response to glial cell line-derived neurotrophic factor or fibroblast growth factor 2. Undifferentiated spermatogonia in vivo exhibited high levels of *Spry4* mRNA. Quantitative single-cell analysis of ERK MAPK signaling in spermatogonial stem cell cultures revealed both dynamic signaling patterns in response to growth factors and disruption of such effects when *Spry4* was ablated, due to dysregulation of ERK MAPK downstream of RAS. Whereas negative feedback regulator expression decreased during differentiation, loss of *Spry4* shifted cell fate toward early differentiation with concomitant loss of stem cell activity. Finally, a mouse *Spry4* reporter line revealed that the adult spermatogonial stem cell population in vivo is demarcated by strong *Spry4* promoter activity. Collectively, our data suggest that negative feedback-dependent regulation of ERK MAPK is critical for preservation of spermatogonial stem cell fate within the mammalian testis.

Summary sentence
The *Spry4* is a novel ERK-dependent negative feedback regulator of FGF and GDNF signaling that is critical for preservation of stem cell activity in cultured adult mouse spermatogonia and serves as a marker for adult SSCs in vivo.

Received: February 15, 2023. **Revised:** June 28, 2023. **Accepted:** August 5, 2023

Graphical Abstract

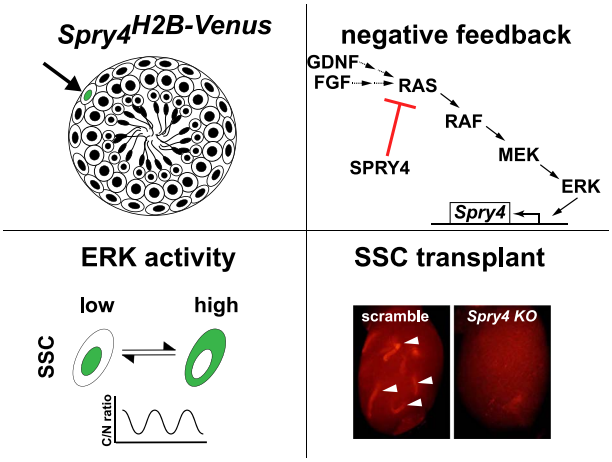

Keywords: spermatogonial stem cells, spermatogonia, ERK MAPK signaling, negative feedback, growth factor signaling

Introduction

Stem cells in adult tissues are essential for maintaining homeostasis. In contrast to classical hierarchical models, accumulating data suggest phenotypic plasticity within undifferentiated cell populations, depending upon the condition of the tissue and whether it is subject to stress [1–5]. Environmental stress together with cell-autonomous deregulation of signaling during aging also alters stem cell and tissue function [6–8]. Yet, the dynamics of signaling pathways that control stem cell fate are opaque.

Spermatogonial stem and progenitor cells (SSCs) of the mammalian testis, which are responsible for perpetuating male gamete production even into advanced paternal age, represent an attractive model to study the mechanisms that regulate stem cell behavior in an adult solid organ with robust cellular turnover. Glial cell line-derived neurotrophic factor (GDNF) and fibroblast growth factors (FGFs) are critical for homeostasis of adult SSCs, a subpopulation of the GFRA1$^+$ undifferentiated spermatogonia (Spg_{undiff}) in vivo [9–12]. Spg_{undiff} comprise isolated single cells (A_{single}) and cells in pairs (A_{pair}) or chains of varying lengths ($A_{aligned}$). Beyond static, morphologic features, evidence from both functional and molecular studies suggests that the adult stem pool is dynamic and not strictly hierarchical [1, 12–14]. The ability to block transduction of niche-mediated signals (e.g. downstream of Wnt/beta-catenin) is thought to be a critical feature within a subset of the GFRA1$^+$ Spg_{undiff} [15].

Techniques to reliably propagate adult mouse SSCs in vitro have led to key insights into their self-renewal, despite the fact that only a minority of cells in culture function as stem cells in transplantation assays [16] and that putative hierarchical relationships within the SSC pool may be abrogated in vitro [14]. Hereafter, we employ the term cultured SSCs to refer to both the adult stem and progenitor populations in vitro, mindful that transplantable stem cells constitute only a small fraction of the population. While it is accepted that GDNF supports mouse SSC self-renewal [9, 17–19], contradictory evidence exists regarding SSC fate outcomes in response to FGF exposure and ERK MAPK pathway activation. Some results indicate that FGF supports self-renewal [20–22], while others suggest that FGF can impair the SSC phenotype [14, 23, 24]. In vivo, FGF availability is a major determinant of the set-point for SSC density [21]. Furthermore, differential responses to GDNF vs. FGF2 are particularly apparent in experiments using cultured SSCs, which are highly dependent upon exogenous GFs [20, 24].

Among the myriad signals that impinge on ERK MAPK, the significance of cytoplasmic negative feedback regulators in stem cells has only recently been explored in depth [6, 25, 26]. Studies in other stem cell model systems indicate that homeostasis is controlled more by the fine-tuning of ERK MAPK signaling downstream of GFs rather than simply whether the pathway is turned on vs. off [27, 28]. Observations from the male germline support the conclusion that expression of negative feedback regulatory genes (e.g., members of the dual specificity protein phosphatase [DUSP] and Sprouty [SPRY] gene families) is associated specifically with SSC-like cell populations across multiple species [14, 21, 29–34]. Yet, relatively sparse attention has been given to the mechanisms of negative feedback control on the MAPK pathway in SSCs and the specific genes involved. Notably, a recent report implicated *Dusp4* in modulation of JNK signaling [35]. Also, aberrant ERK MAPK upstream of mTORC1 was shown to compromise SSCs lacking *Tsc22d3*/GILZ [36].

Members of the SPRY gene family (Spry1–4 in mammals) were originally identified based on their shared C-terminal cysteine-rich domain and ability to inhibit GF-induced ERK MAPK signaling during development [37, 38]. Mammalian SPRY proteins are thought to form cooperative homo- and hetero-oligomers [39]. While multiple potential sites of action of SPRY proteins within the GF-signaling cascade have been reported (e.g., at the level of RAF), some appear to be cell type specific and/or GF specific [38, 40]. In particular, SPRY4 suppresses ERK MAPK activity induced by FGF, but also by vascular endothelial cell growth factor and nerve growth factor in some cell types, and acts at the level of RAS and/or RAF1 depending on the type of GF [40–42].

Herein, we uncovered a growth factor-responsive negative feedback response in SSCs, dependent upon *Spry4*, which is selectively expressed in a subset of undifferentiated spermatogonia in vivo. Following exposure to FGF2 or GDNF, SPRY4 was critical to maintain stem cell activity of cultured SSCs

and modulated the ERK MAPK pathway at the level of RAS or above. Interrogation of a *Spry4*$^{H2B\text{-}Venus}$ transcriptional reporter mouse line demonstrated that *Spry4* expression is a hallmark of adult SSCs.

Materials and methods

Ethics statement

This study was approved by the Weill Cornell Medical College IACUC (#2010-0028). Ketamine/xylazine was used for anesthesia in combination with buprenorphine and meloxicam for analgesia. For euthanasia, mice were exposed to CO_2 followed by cervical dislocation.

Animals

The *Gfra1-creER*^{T2} mice were a gift from Dr. Sanjay Jain [12, 43]. LSL-t*dTomato* reporter mice (#007914) were obtained from the Jackson Laboratory [44]. The ERK-KTR reporter mice (*Hprt*$^{CAG\text{-}ERK\text{-}KTR\text{-}mClover}$;*Rosa26*$^{CAG\text{-}3xNLS\text{-}mKate2}$) [45], *Spry4*$^{H2B\text{-}Venus}$ mice [46], and *Spry4*^{fl} mice [47] were described previously. Tamoxifen (T5648, Sigma-Aldrich) was administered to animals by intraperitoneal injection at a dose of 100 mg/kg of body weight once every 24 h for 3–4 consecutive days per week for 2 weeks total.

SSC lines and cell culture

Primary SSC lines were derived from adult mouse testes and maintained on mitotically inactivated JK1 feeders [48]. Adult donor animals included C57Bl6, mixed C57Bl6/129 mice, and the following strains on a mixed background: *Hprt*$^{CAG\text{-}ERK\text{-}KTR\text{-}mClover}$;*Rosa26*$^{CAG\text{-}3xNLS\text{-}mKate2}$, *Spry4*$^{H2B\text{-}Venus}$, *Spry4*$^{fl/fl}$, and GCRT;Spry^{fl} [45, 46]. SSC cultures were established from freshly dissected testes by two-step enzymatic digestion [48]. Briefly, detunicated testes collected in a sterile fashion were minced and digested at 37°C in two subsequent steps with collagenase I (0.03% wt/vol; CLS-1, Worthington Biochemical) followed by porcine pancreas trypsin (0.05% wt/vol; 27250-018, Gibco). Cell suspensions were plated in six-well plates coated with gelatin (G1890-100G; Sigma-Aldrich) at a density of 1/8 testis per well in 2 ml final volume of cell culture medium (see below) at 37°C in 5% CO_2. Depending on the age and mouse strain, plating densities were varied as needed. Half of the medium was changed after 72 h and every 48 h afterwards preserving at least 1 ml of conditioned medium in each passage. One to four weeks after plating, SSC colonies were manually picked and plated into mitotically inactivated JK1 feeder cells for long-term culture and expansion (Supplementary Figure 1) [49]. Cell culture medium for SSC maintenance (i.e., growth medium) consisted of StemPro-34 (10640, Thermo Fisher Scientific) with nutrient supplement (10641, Thermo Fisher Scientific) plus additional supplements and growth factors at the following concentrations: 20 ng/ml GDNF (PHC7041, Life Technologies, USA), 10 ng/ml FGF2 (PHG0024, Thermo Fisher Scientific), 25 μg/ml human insulin (I9278, Sigma-Aldrich), and 20 ng/ml EGF (PHG0313, Thermo Fisher Scientific). For feeder-free experiments, SSCs and feeders were trypsinized and incubated in plates coated with 4% gelatin (G1890, Sigma-Aldrich) at 37°C/5% CO_2 for 2 h, which enabled collection of the SSCs (floating in the medium), whereas feeders adhered to the plates and were discarded. SSCs, free of feeders, were then re-plated in wells coated with 4% gelatin (G1890, Sigma-Aldrich) or 1% Matrigel matrix (354234, Corning) and maintained in standard cell culture medium (i.e., growth medium) or starving medium (i.e., without FBS and GFs) prior to experiments (see below).

In vitro treatment with growth factors, inhibitors, cytokines, retinoic acid, and tamoxifen

For GF stimulation, feeder-free SSCs were first starved overnight. Treatments were performed for the time points indicated below in starving medium containing the indicated growth factors, cytokines, and/or inhibitors. SSCs were treated for 6 h (Figure 1A and B), 12 h (Figure 1C), 30 min (Figure 2C), 30 or 60 min (Figure 2D), up to 3 h (Figure 2E), 2 days (Figure 3A), 3 days (Figure 3B), 6 days (Figure 3C), up to 6 days (Figure 3D), 3 days (Figure 3F–H), 4 h (Figure 4A), up to 3 h (Figure 4B), 2 h (Figure 4C and D), 2 days (Figure 5A–C), 3 days (Figure 5D and E), 2 days (Supplementary Figure 2A and B), 4 h (Supplementary Figure 3), up to 3 h (Supplementary Figures 5 and 6), or 2 days (Supplementary Figure 8). All experiments except for in vitro differentiation (Figure 5; see below) were performed at 37°C. For differentiation experiments, SSCs were either maintained in growth medium or plated onto gelatin-coated wells without feeders with or without 1 μM retinoic acid (RA; R2625, Sigma-Aldrich) or vehicle control (DMSO; D2650, Sigma-Aldrich) for the time points as indicated above and in figure legends. For Figure 5A–C, SSCs with feeders were switched to 34°C incubator for 2 days (prior to RNA collection) or 3 days (prior to immunostaining) in growth medium or 10% growth medium diluted in 90% Earle's balanced salts solution (E2888, Sigma-Aldrich) [50]. The differentiation medium ("cocktail") included 1 μM RA with 25 ng/ml NRG1 (396-HB-050, R&D Systems) and 50 ng/ml Kit ligand (455-MC-010, R&D Systems), as indicated. For tamoxifen treatment, SSC lines were maintained in growth medium or plated onto gelatin-coated wells without feeders in growth medium and treated with 7 μM 4-hydroxytamoxifen (4-OHT; H7904, Sigma-Aldrich) or corresponding vehicle control for 3–4 days. For testing of pathway inhibitors (Figure 4A), cells were starved overnight and pre-treated for 1 h with the following compounds at the indicated concentrations: PD0325901 MEK inhibitor (1 μM; S1036, Selleckchem), PI3K inhibitor LY294002 (50 μM; 9901S, Cell Signaling), PKC inhibitor GF109203X (5 μM; S7208, Selleckchem), P38 inhibitor SB203580 (10 μM; S1076, Selleckchem), and JNK inhibitor SP600125 (10 μM; S1460, Selleckchem).

Lentiviral transduction

Lentivirus transduction was performed in feeder-free SSC cultures overnight in growth medium containing polybrene (5 μg/ml; TR-1003-G, Millipore), after which cells were transferred onto fresh feeder cells for expansion. CRISPR/Cas9-mediated targeting of SSCs was performed as described previously [51]. The following lentiviruses were purchased from Vectorbuilder, Inc. and handled as per manufacturer's instructions: CRISPR/Cas9 lentivirus targeting *mSpry4* (pLV-U6-sgRNA [*mSpry4* 1673]-EFS-Cas9-2A-puro and pLV-hCas9:T2A:Neo-sgRNA [*mSpry4* 1673]), scramble controls (pLV-hCas9:T2A:Neo-sgRNA [scramble]), *mSpry4* cDNA (pLV-Puro-hPGK>*mSpry4* [NM_011898.2]), and Stra8-H2B-BFP2 (pLV-Neo-Stra8-hH2BC3 [NM_021062.3]*linker/TagBFP2). The target sequence for mSpry4 sgRNA 1673 is AGCAGGAAGGTAACGTCCGA and the scramble sgRNA

target sequence is GTGTAGTTCGACCATTCGTG. The latter served as an infection control. Cells were expanded following transduction and subject to selection with puromycin (400 ng/ml; P8833, Sigma-Aldrich) or neomycin (400 ng/ml; 21810031, Thermo Fisher Scientific) for 1 week. Pooled antibiotic-selected CRISPR/Cas9-targeted were then subject to the T7 endonuclease assay and single cell cloning/expansion for further analysis by PCR and DNA sequencing. CDNA encoding Cre-ERT^2 (Addgene #22776) was cloned into pCCL-PGK to generate a pCCL-PGK-Cre-ERT^2 lentivirus. Transduction efficiency of vectors was monitored by qRT-PCR and immunoblot.

Quantitative reverse transcription polymerase chain reaction

Total RNA was extracted from feeder-free cultured SSCs or sorted spermatogonia isolated by FACS using RNeasy Plus microextraction kit (74034, Qiagen) or Arcturus Pico Pure with on-column DNA digestion (KIT0204, Thermo Fisher Scientific), respectively. RNA was reverse transcribed using qScript cDNA SuperMix (101414-106, Quanta Biosciences). Quantitative reverse transcription polymerase chain reaction (qRT-PCR) was performed in triplicate in a LightCycler 480II Real-Time System (Roche Molecular Systems) using PerfeCta SYBR Green FastMix (4472919, Thermo Fisher Scientific). Primers were validated for use based on efficiency and inspection of melting curves. For quantification, each technical triplicate was normalized to endogenous *Actb* and *Gapdh* and relative transcript expression was calculated using the comparative C_T method ($2^{-\Delta\Delta Ct}$ method) using one of the technical triplicates of the control condition as the reference value. Data presented correspond to *Gapdh* normalization.

Fluorescence-activated cell sorting

To generate samples for cell profiling and transplantation experiments, *Gfra1-CreER^{T2}* mice were first crossed with *Rosa26-LSL-tdTomato* reporter mice [12, 43] and *Spry4$^{H2B\text{-}Venus}$* mice [46]. For fluorescence-activated cell sorting (FACS) for MCAM, a marker of SSCs and spermatogonia [52, 53], testes from *Gfra1-CreER^{T2}; Rosa26-LSL-tdTomato* mice were dissociated ≥3 months after tamoxifen administration. Single-cell suspensions were generated from testes of adult mice by two-enzymatic digestion as described above. Cell suspensions were incubated with Alexa Fluor 647 anti-MCAM antibody (ME-9F1, BioLegend, San Diego, CA, USA) at 6 mg/ml for 45 min at 4°C. Cell suspensions with immunocomplexes were subject to FACS with a BD FACS Aria II instrument (Beckman Coulter, USA). DAPI (D1306, Thermo Fisher Scientific) was used for live/dead cell discrimination. RNA was extracted from sorted cells for QRT-PCR (see below). For analysis of STRA8 and phospho-ERK in cultured SSCs, single-cell suspensions were fixed with 4% paraformaldehyde (158127-500G, Sigma-Aldrich) at 37°C for 10 min. Cells were permeabilized with 90% methanol for 30 min on ice, and incubated with rabbit anti-STRA8 (ab49405, Abcam) at 1:200 dilution or rabbit anti-phospho-p44/42 (ERK1/2,Thr202/Tyr204) antibody (9101, Cell Signaling Technology) at 1:100 for 1 h at room temperature. Cells were resuspended in buffer with donkey anti-rabbit Alexa-488 conjugate antibody (711-545-152, Jackson ImmunoResearch Labs) at 1:1000 dilution for 30 min at room temperature. Cells were analyzed on an Accuri C6 flow cytometer (BD Biosciences).

SSC transplantation

The SSC transplantation assays were performed as described previously using busulfan-conditioned mice [54]. Briefly, C57BL/6J male mice at 6–8 weeks of age were treated with 40 mg/kg of busulfan (B2635, Sigma-Aldrich) and used 4–8 weeks later as recipients by microinjection into the efferent ducts. Fluorescent positive colonies were counted using a fluorescent stereoscope (Nikon, USA) 6–8 weeks after transplantation. For determination of *Spry4$^{H2B\text{-}Venus}$* stem cell activity, a constitutive, ubiquitous *tdTomato* mouse line was generated by treating *Gfra1-CreERT2;Rosa26-LSL-tdTomato* males with tamoxifen and breeding them with C57Bl6 females. Then, *Spry4$^{H2B\text{-}Venus}$;tdTomato* animals were generated by crossing *Spry4$^{H2B\text{-}Venus}$* mice with the constitutive *tdTomato* mouse line. Testes from adult *Spry4$^{H2B\text{-}Venus}$;tdTomato* or GCRT;Venus mice were dissociated as described above to produce single-cell suspensions [46]. A BD FACS Aria II instrument (Beckman Coulter, USA) was used to sort Venus-positive and unselected (control) cells from *Spry4$^{H2B\text{-}Venus}$;tdTomato* mice and Venus-bright Spg_{undiff} and Venus-negative germ cells from tamoxifen-induced GCRT;Venus mice. Briefly, cells were gated for singlets using forward and side scatter, collected, and transplanted (500 000–700 000 cells injected for unselected vs. 10 000–15 000 cells injected for Venus-positive) into busulfan-treated C57Bl6 recipients as above. The TdTomato-positive colonies were counted using a stereo fluorescent microscope at ∼2 months after transplantation. Transplant experiments were repeated three times.

Immunofluorescence staining

Cultured SSCs were fixed with 4% paraformaldehyde (PFA; 158127, Sigma-Aldrich) for 10 min at room temperature (RT, hereafter). Cells were blocked with 3% bovine serum albumin (A1470, Sigma-Aldrich)/phosphate-buffered saline before incubation with 2 μg/ml rabbit anti-SYCP3 (NB300-232SS, Novus Bio), 0.25 μg/ml rat anti-MCAM antibody (134702, BioLegend) or 2 ug/ml normal rabbit IgG (011-000-003, Jackson ImmunoResearch) overnight at 4°C in a humidified chamber. Detection of primary antibodies was performed using Alexa-647 conjugated Anti-Rabbit IgG (711-065-152, Jackson ImmunoResearch) at 1 μg/ml or biotin-SP donkey anti-rat secondary (712-065-153, Jackson ImmunoResearch) then SA-DyLight 405 fluorophore (016-470-084, Jackson ImmunoResearch), respectively, at 1 μg/ml or for 60 min at RT. Slides were counterstained and mounted with Vectashield HardSet Antifade Mounting Medium with DAPI (H-1500, Vector Laboratories, Burlingame, CA, USA) and analyzed using a Zeiss LSM 800 confocal microscope (Carl Zeiss Inc., Thornwood, NY, USA).

For staining of spermatogonia in vivo, testes were freshly collected and fixed in 4% PFA overnight at 4°C and then washed with 1× DPBS (SH30013.03, Thermo Fisher) before being incubated in 30% sucrose (S7903, Sigma-Aldrich) for 48 h at 4°C. Testes were then embedded in Clear Frozen Section Compound (95057-838, VWR, USA) and stored at −80°C before use. Tissue cross-sections at 6 μm thickness were generated using the Leica CM3050S cryostat (Leica Biosystems, Buffalo Grove, IL, USA). Sections were processed

a standard immunofluorescence detection protocol. Briefly, sections were incubated with primary antibody against anti-rat GFRA1 (2.5 μg/ml; AF560, R&D Systems) and detected with Biotin-SP-Donkey Anti-Rat IgG (712-065-153, Jackson ImmunoResearch) at 1 μg/ml for 90 min at RT followed with Streptavidin Alexa Fluor 647 (016-600-084, Jackson ImmunoResearch) at 1 μg/ml for 30 min at RT. For MCAM staining, sections were incubated overnight at 4°C with rat anti-MCAM antibody (134702, Biolegend) at 0.25 μg/ml followed by Biotin-SP Anti-Rat IgG (712-065-153, Jackson ImmunoResearch) at 1 μg/ml for 90 min at RT and then Streptavidin Alexa Fluor 555 (S-21381, Thermo Fisher Scientific) at 1 μg/ml for 30 min at RT. Sections were then mounted and counterstained with VECTASHIELD HardSet Antifade Mounting Medium with DAPI (H-1500, Vector Laboratories). For whole-mount immunofluorescence of seminiferous tubules, freshly collected testes were fixed in cold 4% PFA without tunica albuginea for 14 h. The tubules were isolated, blocked in 3% BSA/PBS with 0.1% Tween-20 (P7949, Thermo Fisher Scientific), and incubated with anti-GFRA1 antibody (2.5 μg/ml; AF560, R&D Systems) overnight. Biotinylated secondary antibodies followed by Alexa647-streptavidin were used for detection (see below).

Confocal image acquisition, live imaging, and quantification

Imaging of fixed tissue and live cells was performed on a Zeiss LSM800 confocal microscope. Time-lapse imaging experiments were performed in 35-mm glass-bottomed dishes (627975, Greiner). To improve cell adherence and viability, before plating, the bottom of each well was pre-treated with a solution of 1% Matrigel matrix (354234, Corning). Then feeder-free ERK-KTR-SSCs were seeded at 600 000–800 000 cells/well in 600 μl SSC medium. The cells were allowed to adhere overnight before imaging. All time-lapse images were captured with a 488-nm laser for ERK-mClover and a 561-nm laser for NLS-mKate2 using a 20× objective in a humidified incubation chamber with 5% CO_2 at 37°C. The C/N (cytoplasmic to nuclear ratio) of ERK-mClover intensity served as the primary read-out of ERK activity using this reporter. Nuclear and cytoplasmic regions of each cell were segmented, tracked, and measured computationally with Imaris (Bitplane) using the cell module function to calculate the C/N ratio at a single-cell level. First, the NLS-mKate channel was used to define cells as objects and perform nuclear segmentation. Cells and nuclei were classified by manually setting the threshold of the expected diameter and intensity. Next, the cell bodies and cytoplasmic regions were detected using the arithmetically combined NLS-mKate and ERK-mClover channels. Cells were then classified by adding filters to restrict the set based on cell size, nuclear size, one nucleus per cell, and track length. Finally, tracking filters were set, including the track length and the maximum distance, and then the nuclei and cells were tracked over the entire course. All measurements of the nuclear and cytoplasmic regions for each single cell in each tracked time point were exported for further analysis.

Analysis of dynamic time course live imaging data using Matlab

The ERK pulsatile analysis was performed in Matlab R2018a. Peaks were identified using findpeaks module with the time course quantified traces dataset by the above Imaris. After the traces were smoothened using smoothdat to reduce noise for peak calling, the threshold for the peak prominence was set based on values obtained from negative controls, including a MEK inhibitor-treated condition (to suppress ERK signaling) and a starved condition (without FBS and GFs) to detect background ERK-dependent pulses. Prominence was defined as the peak value maxima relative to the nearest local minima. The amplitude was defined as local peak value between local minima. Duration was the width at half prominence. Finally, all the measurements of the peak amplitude, prominence, duration in each identified peak, and the peak number or frequency in the single-cell trace level were exported for analysis.

Immunoblot and active RAS detection

Feeder-free SSCs were suspended in lysis buffer RIPA Buffer (89900, Thermo Fisher Scientific) and protease and phosphatase inhibitors cocktails (P5726, Thermo Fisher Scientific). Total cell lysates were separated by SDS-PAGE and transferred into a PVDF membrane (162-0177, BioRad Laboratories). Membranes were blocked in Tris-buffered saline containing 0.1% Tween-20 (TBST) with 5% BSA and incubated with the following primary antibodies: SPRY4 (PA5-26959, Thermo Fisher); phospho-p44/42 MAPK (ERK1/2) (Thr202/Tyr204) (#9101) and p44/42 MAPK (ERK1,2) (#9102) from Cell Signaling Technology; DUSP6 (ab76310, Abcam), GAPDH (ab9484, Abcam), PPIB (PA1-027A, Thermo Fisher), and TUBULIN (2146S, Cell Signaling) were used as loading controls. Blots were washed with TBST and incubated at room temperature with the appropriate secondary antibody conjugated to horseradish peroxidase. Chemiluminescent immunodetection was performed with ECL system (32209, GE Healthcare BioSciences), and membranes were exposed to X-ray film and digitized scans of the blots were analyzed using ImageJ (National Institutes of Health) for densitometry. Active RAS was specifically pulled down from lysates from cultured SSCs using the Active RAS Pull-Down and Detection Kit with the GST-fusion protein of the RAS-binding domain of RAF1 along with glutathione agarose resin according to the manufacturer's protocol (16117, Thermo Fisher) and detected by immunoblot as described previously [55].

Single-cell mRNA sequencing

Spermatogenic stem cells (SSCs) were isolated from *Gfra1-CreER^{T2};Rosa26-LSL-tdTomato;Spry4$^{H2B\text{-}Venus}$* mice as follows. Three adult males were sacrificed 18 days after the first dose of tamoxifen, which was given four consecutive days per week for two consecutive weeks (100 mg/kg of body weight once every 24 h). Dissociated cells from bilateral testes were isolated by flow cytometry and gated based on double positivity for tdTomato and Venus. An input sample (~16 500 cells; expected recovery rate ~65%, excluding non-viable cells and doublets) was captured in droplet emulsions using a Chromium Single-Cell instrument (10x Genomics), and the library was prepared using the 10x Genomics 3′ single-cell V3 protocol. The 10x libraries were pooled and sequenced on an Illumina NovaSeq 6000 instrument.

Reads from single cells were aligned to the mouse reference genome mm10-2020-A (GENCODE vM23/Ensembl 98) using Cell Ranger (version 3.0.2, 10x Genomics) as follows. The raw sequencing data generated from the scRNA-seq experiment were first demultiplexed using the cell barcodes and unique molecular identifiers (UMIs) to assign reads to individual cells, using CellRanger Single-Cell Software Suite

(V3.1.0). Next, the demultiplexed reads were aligned to the reference genome using the STAR aligner, which mapped the reads to the genome and accounted for splicing events and gene isoforms. After alignment, the UMIs and cell barcodes were used to generate counts for each gene in each cell. This involved collapsing identical UMIs within a cell and discarding any UMIs that mapped to multiple genes. The resultant raw expression data identified a total of 9996 cells, with 20 294 mean reads per cell. Quality filtering was performed Seurat 4.0.0 [56] and scater 1.20.0 [57]. First, we removed outlier cells at 3 median absolute deviations (MADs) below the median gene number per cell, the median transcript number per cell, and at 3 MADs above the median mitochondrial RNA percentage. Then, we excluded low-quality cells with <1000 detected genes or <3000 detected transcripts, or >15% mitochondrial RNA percentage. After removing low-quality cells, 9455 high-quality cells remained, with a mean of 10 048 transcripts per cell and 3316 genes per cell.

Dimension reduction of single-cell mRNA sequencing data

Gene expression counts were normalized, log-transformed by SCTransform in the R software package Seurat 4.0.0 [56]. The top 2000 variable genes were used to prepare the scaled data and used to calculate the principal components. The top 25 principal components were selected to generate a Uniform Manifold Approximation and Projection (UMAP). Clusters of similar cells are detected using the original Louvain algorithm and UMAP coordinates to construct a shared nearest neighbor graph by "FindNeighbors" function.

Cell-type identification in scRNA-seq data

A two-step cell-type identification was performed to annotate every single cell. First, the SingleR package [58] was leveraged, using single-cell spermatogonial and spermatocyte data [59] as a reference database to annotate each cell. SingleR calculated the Spearman coefficient between every single-cell gene expression and each pure cell-type reference data set. This process was performed iteratively until only one cell type remained with the highest coefficient. This allowed us to identify 9265 spermatogonia cells, 21 early spermatocytes, 60 round spermatids, 36 spermatocytes, 34 spermatids, 17 other cell types, and 22 unknown cells. Second, later developmental stage cells and others were removed, only keeping the spermatogonia. Two cell cycle scores were calculated—S.Score and G2M.Score—for each cell. Scaled data were then prepared by regressing out the cell cycle scores. Then, the above dimension reduction procedure was repeated and new UMAPs regenerated with the same settings. Then, each subtype of spermatogenic stem cells was manually annotated based on markers. In total, 1842 early SSCs ($MCAM^{high}/Id4^{high}/Gfra1^{high}$), 2048 late SSCs ($MCAM^{medium}/Id4^{medium}/Gfra1^{medium}$), and 5349 $MCAM^{low}/Id4^{low}/Gfra1^{low}$ spermatogonia, comprising 1862 Spg1 ($Sox3^{low}/Nanos3^{low}/Kit^{low}/Stra8^{low}$), 1570 Spg2 ($Sox3^{high}/Nanos3^{high}/Kit^{low}/Stra8^{low}$), and 1917 Spg3 ($Sox3^{low}/Nanos3^{low}/Kit^{high}/Stra8^{high}$), were obtained as described in Figure 6D and E.

Constructing cell development trajectories

To investigate the developmental trajectories of cells across multiple time points, and order them in pseudotime, the algorithms implemented in the Monocle3 package were used [60]. Monocle3 applied a reversed graph embedding algorithm to learn the sequence of gene expression changes and construct single-cell trajectories then reconstructed a "branched" trajectory if there were multiple outcomes of the dynamic biological process. These branches correspond to cellular "decisions." The $k = 13$ nearest neighbor graph was carefully selected for Leiden community detection. The scripts used for analysis and generating figures are available online (https://github.com/nyuhuyang/scRNAseq-SSC).

Statistical analyses

Results are presented as means ± SD or means ± SEM as indicated in the figure legends. At least three biological replicates and three technical replicates were performed for each experiment unless otherwise indicated in the text. The statistical significance was determined with GraphPad Prism (GraphPad Software, La Jolla, CA, USA), version 7.0, using the indicated test in each figure. Results were considered significant at p value <0.05.

Primer sequences for QRT-PCR

Mouse *Actb*
Fwd 5′-GAGAAGATCTGGCACCACACC-3′
Rev 5′-GGTCTCAAACATGATCTGGGTC-3′
Mouse *Gadph*
Fwd 5′-CTAACATCAAATGGGGTGAGG-3′
Rev 5′-CGGAGATGATGACCCTTTTG-3′
Mouse *Gfra1*
Fwd 5′-AGCAACAGTGGCAATGACCTG-3′
Rev 5′-AGTGGTAGTCGTGGCAGTGG-3′
Mouse *Stra8*
Fwd 5′-TCCCAGTCTGATATCACAGC-3′
Rev 5′-TCCCATCTTGCAGGTTGAAGG-3′
Mouse *Kit*
Fwd 5′-GCCAGTGCTTCCGTGACATT-3′
Rev 5′-TGCCATTTATGAGCCTGTCGTA-3′
Mouse *Sohlh1*
Fwd 5′-TCAGAGCTGCTGGAGAGACC-3′
Rev 5′-CCAGGAACAATGTCACTTGC-3′
Mouse *Ret*
Fwd 5′-GGCTGTCCCGAGATGTTTATG-3′
Rev 5′-GACTCAATTGCCATCCACTTGA-3′
Mouse *Id4*
Fwd 5′-ACTACATCCTGGACCTGCAG-3′
Rev 5′-TGCTGTCACCCTGCTTGTTC-3′
Mouse *Sohlh1*
Fwd 5′-TCAGAGCTGCTGGAGAGACC-3′
Rev 5′-CCAGGAACAATGTCACTTGC-3′
Mouse *Dusp2*
Fwd 5′-GTGTGCTTCTTGCGAGGCGG-3′
Rev 5′-TCCACAGGACCACCCTGGTC-3′
Mouse *Dusp3*
Fwd 5′-GTGGGCAACGCGTCTGTGGC-3′.
Rev 5′-TAGGTGATGCCAGAATCCTCG-3′.
Mouse *Dusp4*
Fwd 5′-CCATCGAGTACATCGACGCAG-3′
Rev 5′-AAGCCTCCTCCAGCCTCACC-3′
Mouse *Dusp6*
Fwd 5′-TCATAGATGAAGCCCGAGGC-3′
Rev 5′-GTCGTAAGCATCGTTCATGGAC-3′
Mouse *Dusp9*
Fwd 5′-TCATTGATGAGGCCTTGTCGC-3′

Rev 5′-TCGTTGAGTGAGAGGTGAAGC-3′
Mouse *Nf1*
Fwd 5′-TGTCAACAGGAAGAGCAGCGC-3′
Rev 5′-TCTGCAGCCTGGCCATCTTCC-3′
Mouse *Spry1*
Fwd 5′-CAAGATCAGCCGGCGTGGCG-3′
Rev 5′-CCCGCTCCACAGCACCGTCC-3′
Mouse *Spry2*
Fwd 5′-GCCGCGATCACGGAGTTCAG-3′
Rev 5′-ACC TGC TGG GTA AGG GCA TC-3′
Mouse *Spry4*
Fwd 5′-TGCGTCAAGCTGGCCCAGCG-3′
Rev 5′-CAG ACC TGC TGG TCT TGG TG-3′
Mouse *Spred1*
Fwd 5′-TCTCTAGGGTGCCCAGCGTC-3′
Rev 5′-GCTGACTGAATGGTATCTGGC-3′
Mouse *Dmc1*
Fwd 5′-ATCGGGATTCCAAGATGATG-3′
Rev 5′-TGCAGAGGGCTCTTCTTGTT-3′
Mouse Sycp3
Fwd 5′-ACATGGAAAGAAAAGATCTGCTG-3′
Rev 5′-CTGGCTTTGAAAGAAGCTTTG-3′

Results

Selected negative feedback regulators of ERK MAPK are induced in cultured adult SSCs in response to FGF2 and GDNF

SSCs in vitro comprise a heterogeneous population within which a minority of cells retain regenerative capacity upon transplantation and for which self-renewal depends upon exogenous factors, including recombinant FGF2 and GDNF [61, 62]. To understand how the ERK MAPK signaling axis is regulated in SSCs, we explored negative feedback genes that maintain signaling within a narrow physiological range [63]. Candidate genes were selected from a pool of known ERK MAPK negative regulators, based on previously reported expression in SSCs [14, 29, 31, 64], as well as from the GEO Profiles database, including genes for which expression was stimulated in self-renewal conditions (i.e., in response to GDNF; https://www.ncbi.nlm.nih.gov/geoprofiles/). Such NFRs typically act rapidly to prevent pathway hyperactivation and also are transcriptionally induced by the same upstream signals [65]. For these experiments, we employed SSC lines derived from adult mice as described previously [51]. Among the genes tested, *Spry4* and *Dusp6* were significantly induced by FGF2 stimulation in a cell-autonomous manner (i.e., in the absence of feeder cells; Figure 1A). These results are consistent with a recent report that described the FGF-dependent gene expression program of SSCs [21]. Whereas epidermal growth factor (EGF) failed to induce *Spry4* or *Dusp6*, treatment with GDNF, the prototypical driver of mouse SSC self-renewal, also induced both transcript and protein (Figure 1B and C). Our findings raised the possibility that *Spry4* and *Dusp6* comprise a growth factor-stimulated negative feedback system unique to the SSC population among adult germ cells.

Spry4 expression marks undifferentiated spermatogonia in vivo

To determine whether expression levels of negative feedback regulators correlate with specific populations of germ cells in vivo, we isolated undifferentiated spermatogonia (Spg_{undiff}) from freshly dissociated mouse testicular cells (Figure 1D). Robust cell-surface MCAM expression has been employed previously to select Spg_{undiff} [52, 53]. However, we noted that MCAM is detectable by immunofluorescence not only in germ cells but also somatic cells, which could contribute mRNA to MCAM-positive sorted pools (Figure 1E). In order to obtain a population of MCAM-positive germ cells, devoid of somatic cells, we combined MCAM labeling with adult lineage tracing in vivo by means of a Spg_{undiff} promoter-driven inducible Cre [12]. To that end, we first crossed *Gfra1-CreER*^{T2} mice with *Rosa26-lox-stop-lox(LSL)-tdTomato* animals (referred to hereafter as GCRT mice) [55]. As expected, tamoxifen-treated GCRT offspring had robust tdTomato expression only in germ cells within the testis and served as a source of donor cells for MCAM staining to isolate the $MCAM^{bright}$ phenotypic Spg_{undiff} by FACS (Figure 1F and G). Quantitative RT-PCR showed that this approach exponentially enriched for *Gfra1* expression in the $MCAM^{bright}$ fraction, validating the cell phenotype generated by this strategy (Figure 1H). Robust expression of *Spry4*, as well as *Dusp6*, was found in the $MCAM^{bright}$ phenotypic Spg_{undiff}, compared to $MCAM^{medium}$ or $MCAM^{dim}$ populations. Furthermore, when we compared our data with a previously published dataset (GEO: GSE75532, 15), we confirmed significantly higher levels of *Spry4* (and *Dusp6*) transcripts in the $GFRA1^+$ population in vivo, in comparison to the $Ngn3^+/KIT^-$ and $Ngn3^+/KIT^+$ populations (Figure 1I). Taken together, these data indicate that *Spry4* and *Dusp6* mRNA levels are inversely correlated with the degree of differentiation of Spg_{undiff}.

An ERK kinase translocation reporter enables quantification of ERK dynamics in single live spermatogonia

NFRs, such as *Spry4* and *Dusp6*, are defined in the literature based on several features: (i) transcriptional inducibility by specific pathways (e.g., ERK MAPK) and (ii) inhibitory effects on those same pathways [66]. However, ERK MAPK has been challenging to measure in single SSCs, and most studies have provided only population-averaged measures of signal (e.g., by immunoblot). Flow cytometry has also been used to correlate increasing phospho-ERK levels as SSCs progress from quiescent to active to very early differentiating states [34]. In contrast to immunolabeling, genetic biosensors, including kinase translocation reporters (KTRs), can be used to quantify signaling over time in single cells [67]. We sought to utilize an ERK-KTR to measure fine-scale changes in ERK signaling in SSCs over time, as an alternative to comparatively insensitive antibody-based approaches. Thus, we derived adult SSC lines from *Hprt*$^{CAG\text{-}ERK\text{-}KTR\text{-}mClover}$;*Rosa26*$^{CAG\text{-}3xNLS\text{-}mKate2}$ mice [45] (referred to as ERK-KTR SSCs), bearing ubiquitous expression of both a stable nuclear-localized marker and a dynamic reporter of ERK that shuttles from the nucleus to the cytoplasm in response to phosphorylation by ERK (Figure 2A and B). As with other adult SSC lines in this study, the presence of stem cell activity in long-term cultures was confirmed by transplantation into busulfan-treated recipients (data not shown). To validate the function and specificity of the ERK-KTR in SSCs, cells were re-plated in feeder-free conditions, starved, and treated with FGF2. Whereas FGF2 induced a rapid translocation of the KTR from nucleus to cytoplasm, this was blocked only by an inhibitor of MEK (upstream of

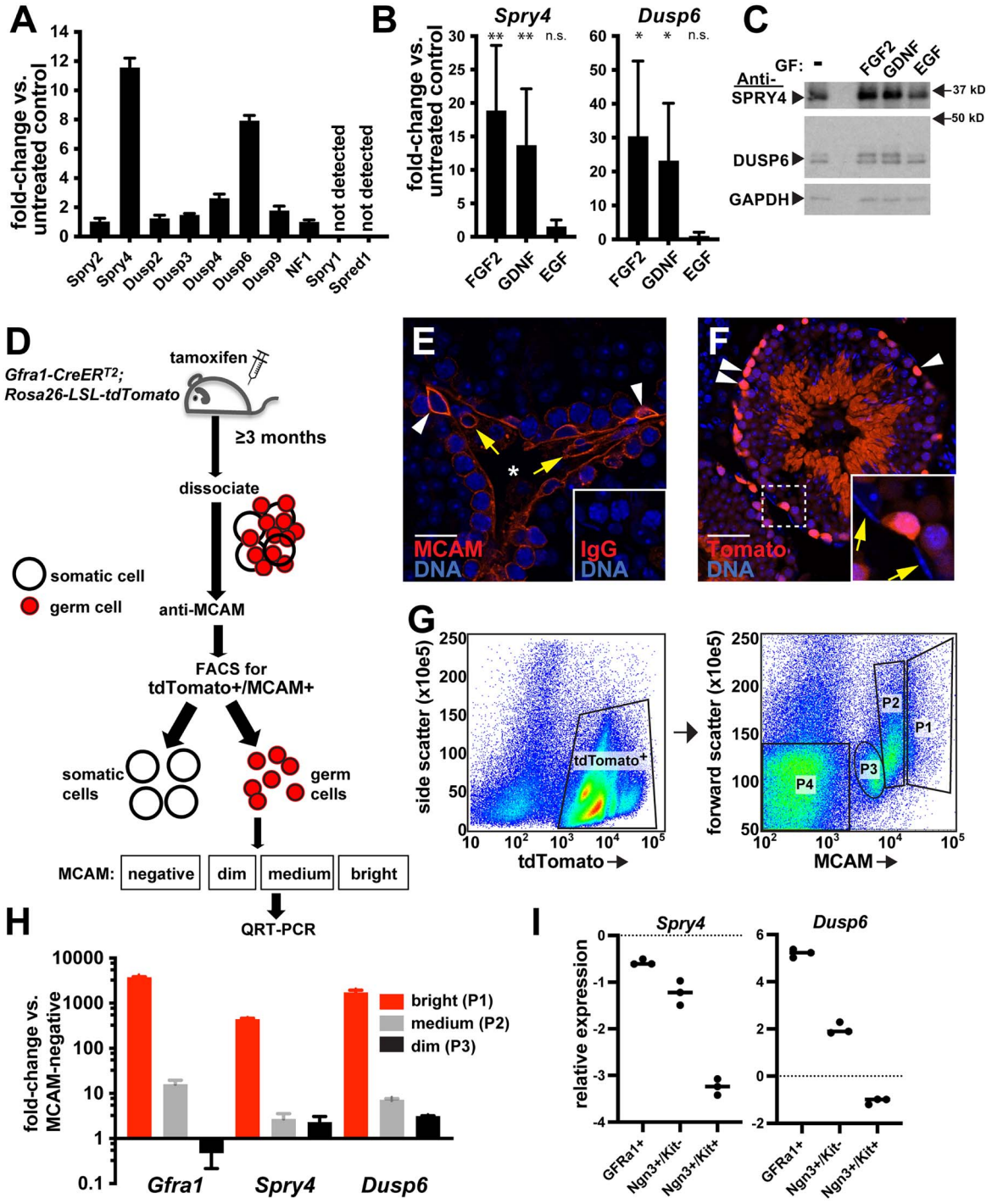

Figure 1. The GF-driven negative regulators of the ERK pathway mark undifferentiated spermatogonia. (A) Representative qRT-PCR showing expression levels of candidate negative feedback genes in response to FGF2 (10 ng/ml), after 6 h of stimulation in comparison to control (mean ± SD of technical replicates; *Spry4*, *Dusp6*, and *Dusp4* vs. control: $p < 0.001$; unpaired *t*-test; $n = 3$ biological replicates). (B) Pooled QRT-PCR data showing induction of *Spry4* and *Dusp6* at 6 h in response to FGF (10 ng/ml), GDNF (10 ng/ml), and EGF (20 ng/ml; mean ± SD; $n = 3$ experiments; *Spry4:* FGF2 and GDNF vs. control: $^{**}p < 0.01$; EGF, n.s.; *Dusp6*: FGF2 and GDNF vs. control $^{*}p < 0.05$; EGF, n.s.). (C) SPRY4 and DUSP6 protein expression by immunoblot in starved or GF-stimulated SSCs after 12 h of stimulation. Arrows indicate molecular weight markers. One representative immunoblot out of three experiments is shown. (D) Schematic of lineage tracing/MCAM FACS strategy to enrich Spg_{undiff} from fresh testis. Adult *Gfra1-CreER^{T2}*; *Rosa26-lox-stop-lox-tdTomato* animals were pulsed with tamoxifen and sacrificed >3 months later to obtain tdTomato-labeled germ cells of all stages. (E) MCAM immunostaining (red) of mouse testis. Arrowheads = MCAM-positive spermatogonia. Arrows = MCAM-positive somatic cells. Asterisk = interstitial space. Inset = IgG control. Size bar = 20 μm. (F) Histologic image depicts efficient tdTomato labeling of only germ cells (arrowheads) since the *Gfra1* promoter is inactive in somatic cells. Inset = unlabeled somatic cells (arrows) as internal control. Size bar = 50 μm. (G) Cell suspensions were labeled with anti-MCAM and sorted into tdTomato-positive fractions with varying MCAM intensity (P1–P3 and P4[MCAM-negative]). (H) qRT-PCR showing gene expression in $MCAM^{bright}$ vs. $MCAM^{medium}$ or $MCAM^{dim}$ germ cells normalized to $MCAM^{negative}$ germ cells (mean ± SD of technical replicates; $n = 3$ biological replicates; unpaired *t*-tests). (I) Relative expression of *Spry4* (left) and *Dusp6* (right) mRNA from Tokue et al. [15] in sorted $GFRA1^{pos}$ vs. $NGN3^{pos}/KIT^{neg}$ and $NGN3^{pos}/KIT^{pos}$ populations. *Spry4* adjusted *p*-val = 0.0036522; *Dusp6* adjusted *p*-val = 0.00000759.

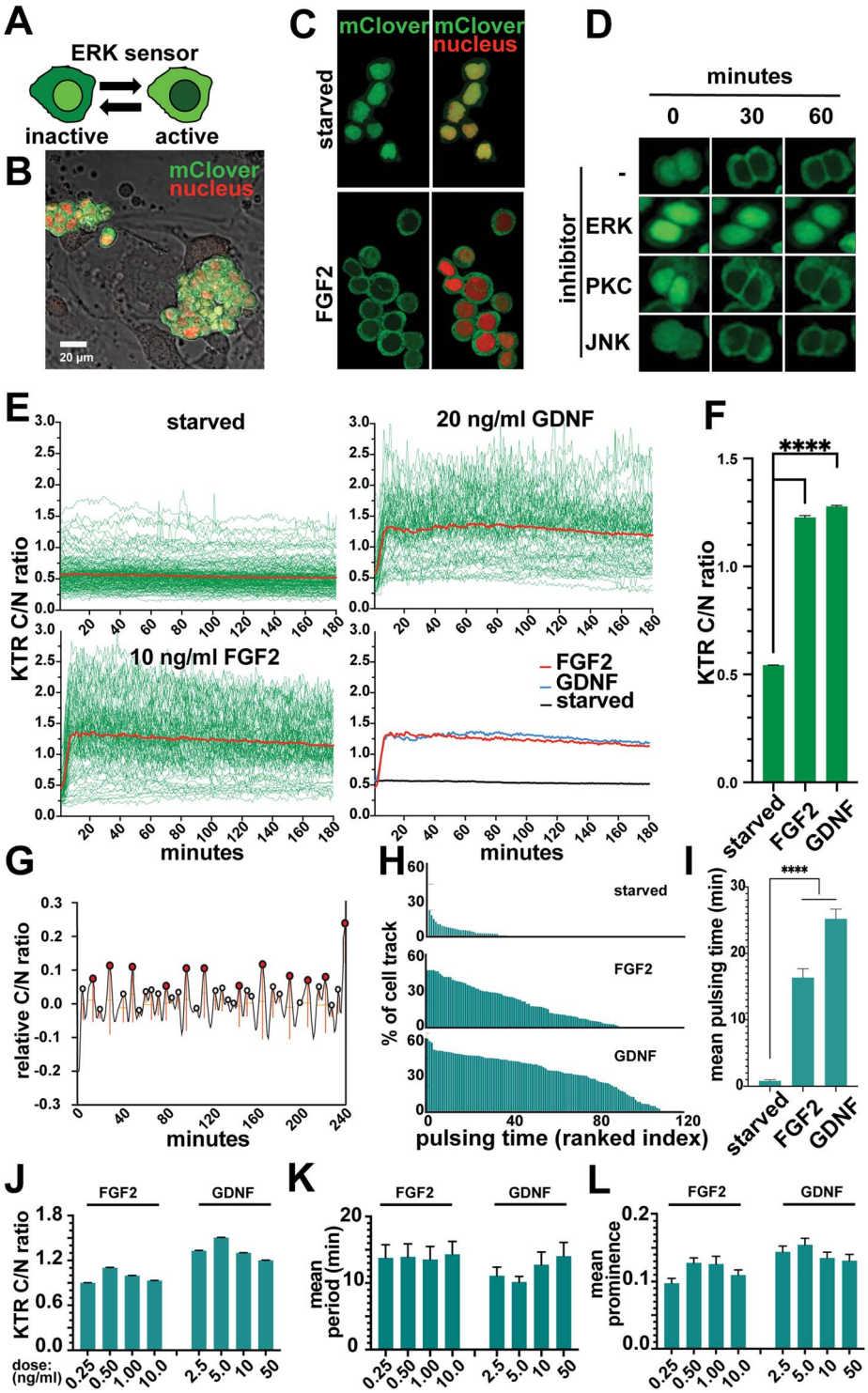

Figure 2. KTR biosensor enables quantification of ERK dynamics in single live spermatogonia. (A) Schematic of ERK-KTR biosensor in SSCs, showing predominant signal in nucleus (inactive) vs. cytoplasm (active). (B) Representative colonies of ERK-KTR SSCs in maintenance culture on feeders (green = mClover ERK biosensor; red = mKate nuclear marker). (C) Representative micrographs of starved SSCs with or without treatment for 30 min with FGF2 1 ng/ml. (D) Time course images of ERK-KTR SSCs following treatment with FGF2 1 ng/ml in the presence or absence of indicated pathway inhibitors, showing inhibition of translocation only by an inhibitor of MEK (upstream of ERK). (E) Representative single-cell tracings green (and population averages [red]) in time course experiments following treatment with FGF2 or GDNF. (F) Summary, population-averaged data for entire time course (all cells and time points) for data from panels shown in (E). (G) Representative single-cell tracing of C/N ratio after smoothing, showing duration (i.e., width [horizontal orange lines]) of annotated peaks (red circles) defined as having prominence (i.e., height) >0.1. Data were then used to calculate pulse period (frequency) and fraction of time spent by each cell pulsing out of the total cell track length. (H) Histogram showing ranked index of pulsing time for the entire time course for all cells following acute stimulation with GFs (starved control, FGF2 [10 ng/ml], or GDNF [20 ng/ml]). (I) Acute stimulation: summary data for pulsing time averaged over all cells/time points (Student's *t*-test, $p < 0.005$ vs. starved). (J–L) Summary data averaged over all cells/time points for chronic stimulation (i.e., maintenance of cell without starvation) in media with FGF2 or GDNF at indicated doses (panel J shows C/N ratio; K, pulse period; and L, pulse prominence).

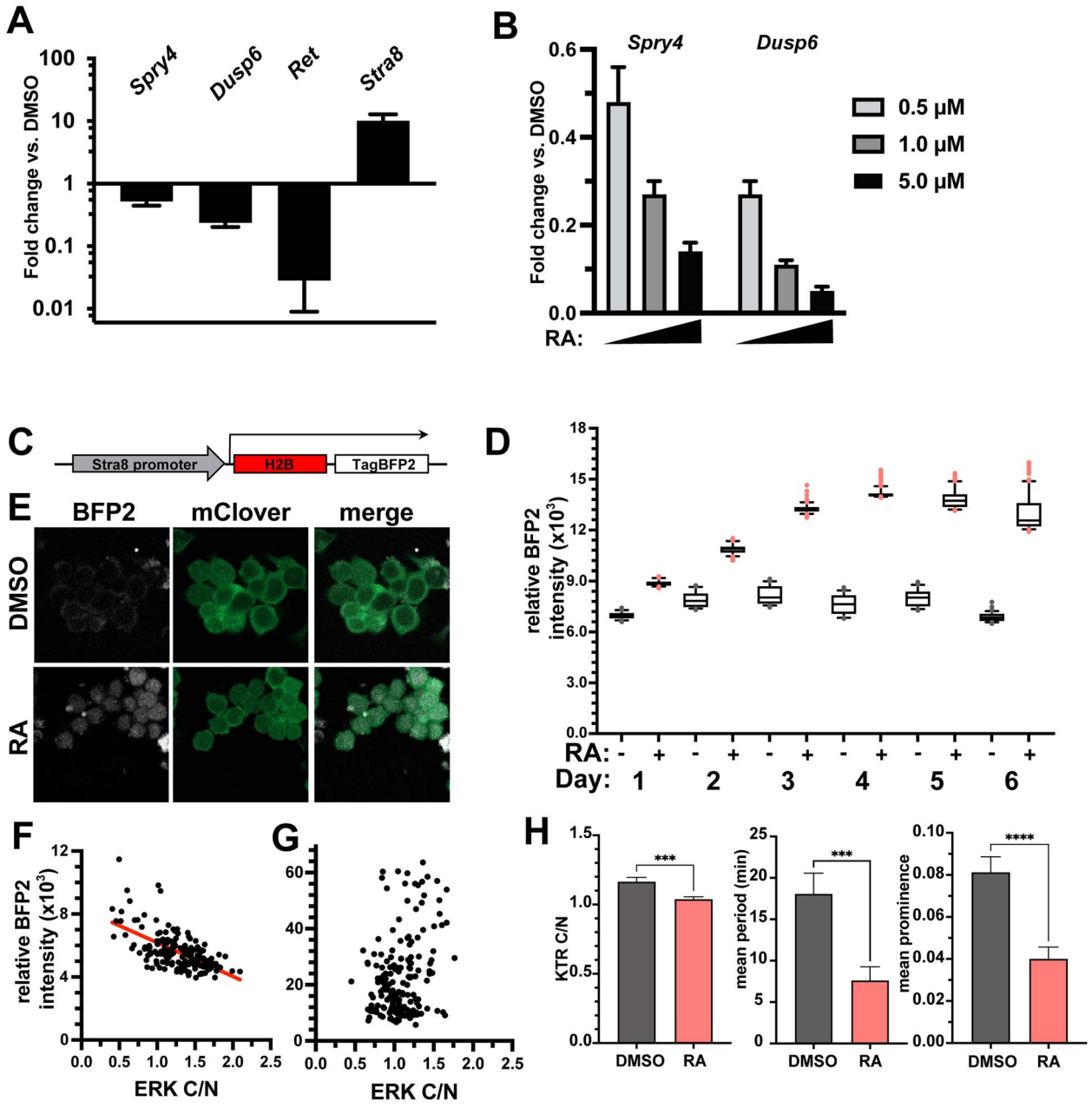

Figure 3. ERK signaling patterns are altered as spermatogonia transition during early differentiation. (A) qRT-PCR for indicated genes following treatment with RA (1 μM) for 2 days (mean ± SD; $n = 3$ biological replicates). (B) qRT-PCR for indicated genes following treatment with RA at 0.5, 1.0, and 5.0 μM for 3 days (mean ± SD; $n = 3$ biological replicates). (C) Schematic of lentiviral *Stra8-H2B-BFP2* differentiation reporter construct. (D) BFP2 intensity in the presence of RA (1 μM) or vehicle (DMSO) over 6 days of treatment. (E) Representative images showing BFP2 and mClover intensities in the presence of RA (1 μM) or vehicle (DMSO) at day 3 of treatment. (F, G) Scatterplots showing BFP2 fluorescence intensity vs. The ERK C/N ratio in single cells treated with FGF2 (1 ng/ml), GDNF (5 ng/ml), and either DMSO (F) or RA (G) for 3 days. (H) Summary data averaged over all cells/time points following 3 days of treatment with RA (1 μM) for KTR C/N ratio (left), pulse period (middle), and pulse prominence (right).

ERK) but not by inhibitors of other major pathways (i.e., PKC or JNK), consistent with findings from other cell types (Figure 2C and D) [45, 67].

To obtain quantitative, dynamic measurements of the acute ERK MAPK response to FGF2 and GDNF for statistical analysis, we collected high-frequency measurements (i.e., ~1 image/minute) following starvation and GF treatment (Figure 2E and F). After automated nuclear and cytoplasmic segmentation of cell images, these data revealed robust activation of ERK in response to either GF, expressed as the ratio of cytoplasmic:nuclear signal (C/N ratio). Notably, traces of ERK-KTR behavior in single cells revealed substantial fluctuations over time, raising the possibility of pulsatile ERK activity in SSCs, as reported in other cell types [28, 68]. To analyze ERK waveforms, we employed peak-calling scripts and collected data on multiple parameters, including pulse period, duration (width), prominence (height), and percentage of time spent pulsing (Figure 2G). Broadly similar dynamic profiles were obtained at doses of either FGF2 or GDNF that yielded maximal ERK MAPK activity, though

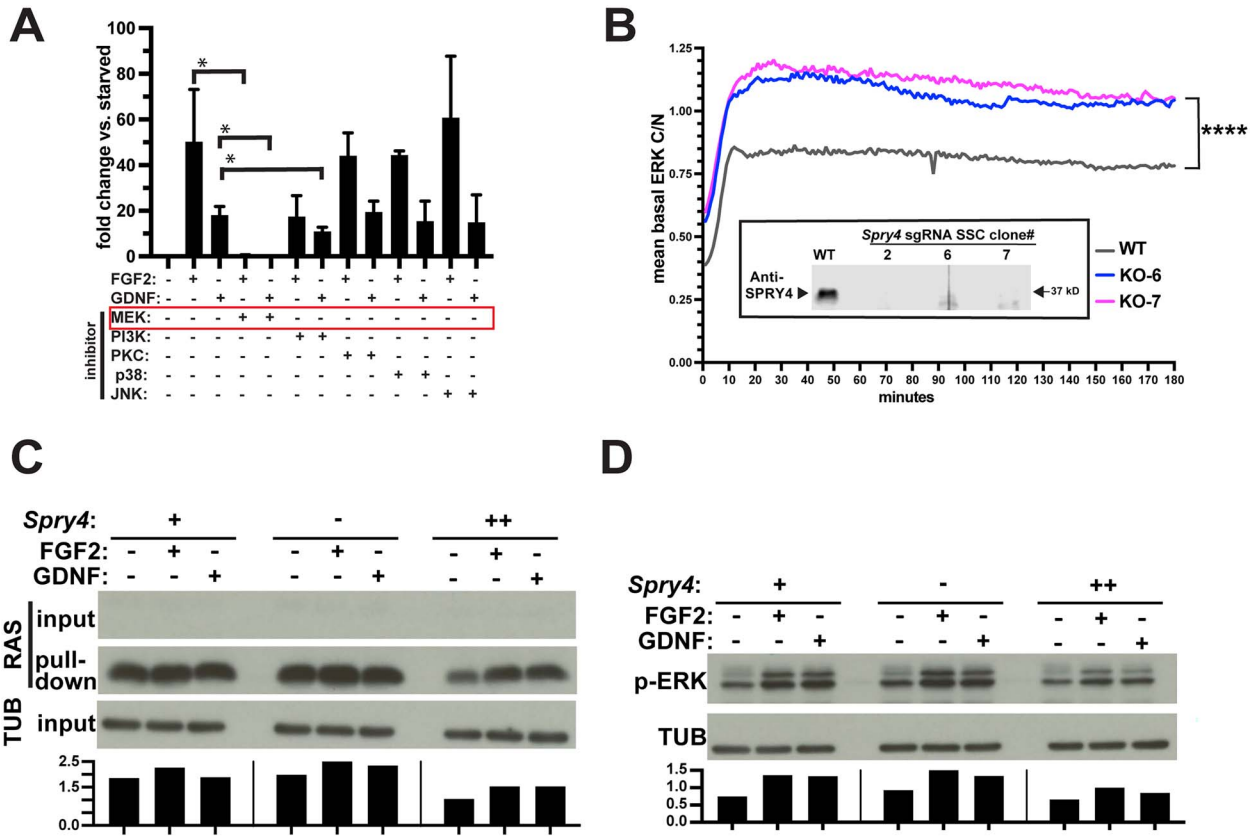

Figure 4. SPRY4 functions as a negative feedback regulator downstream of RAS/RAF/MEK/ERK cascade. (A) Representative qRT-PCR on SSCs (ERK-KTR line) showing *Spry4* induction following starvation and stimulation for 4 h with FGF2 (1 ng/ml) or GDNF (10 ng/ml) in the presence or absence of indicated pathway inhibitors (mean ± SD of technical replicates; $n = 3$ experiments). *T*-test for comparisons± indicated inhibitors: FGF2 vs. FGF2/MEK ($^*p < 0.05$), FGF2 vs. FGF2 with all other inhibitors (p = not significant [n.s.]), GDNF vs. GDNF/MEK ($^*p < 0.05$), GDNF vs. GDNF/PI3K ($^*p < 0.05$), and GDNF vs. GDNF with all other inhibitors (p = n.s.). (B) C/N ratio in CRISPR/Cas9 *Spry4* KO or wildtype (WT) control ERK-KTR SSCs following starvation and acute stimulation with FGF2 (1 μg/ml). Inset shows immunoblot confirming loss of SPRY4 in ERK-KTR SSC subclones (scr = wildtype scramble control). Two *Spry4* KO clones and one WT control (scramble gRNA) clone were tested (one representative experiment out of three is shown; *t*-test, $^{****}p < 0.0001$ for 60-, 120-, and 180-min time points). (**C**) Representative anti-RAS immunoblot showing active RAS pull-down using RAS-binding domain of RAF1 after treatment for 2 h with vehicle, FGF2 (1 μg/ml), or GDNF (10 μg/ml) in SSCs (C57Bl6): control ("*Spry4* +"), *Spry4* deficient SSCs ("*Spry4* −"), or *Spry4* overexpressing SSCs ("*Spry4* ++"). Graphs at bottom depict relative intensity of RAS normalized to TUBB (one representative experiment shown; $n = 2$ biological replicates). (D) Immunoblot on CRISPR/Cas9 *Spry4* KO SSCs (C57Bl6) showing anti-p-ERK (Thr202/Tyr204) after treatment for 2 h with vehicle, FGF2 (1 μg/ml), or GDNF (10 μg/ml) in control SSCs ("*Spry4* +"), *Spry4* KO SSCs ("*Spry4* −"), or *Spry4* overexpressing SSCs ("*Spry4* ++"). Graphs at bottom depict relative intensity of RAS normalized to TUBB (one representative experiment shown; $n = 2$ biological replicates).

GDNF exhibited a more robust average C/N ratio and greater time spent pulsing (Figure 2H–L). These data demonstrate the utility of the ERK-KTR sensor for revealing detailed dynamics of ERK behavior in both individual cultured SSCs and populations.

ERK signaling patterns are altered during early differentiation

Retinoic acid (RA) has been shown to drive differentiation commitment in the subset of Spg_{undiff} in vivo that possess the ability to respond to RA and also drives early in vitro differentiation [69–72]. Given the association between ERK MAPK activity and SSC self-renewal and our observation that *Spry4* and *Dusp6* transcripts were correlated with the Spg_{undiff} phenotype in vivo, we tested the response of cultured SSCs to RA. As expected, mRNAs for *Spry4*, *Dusp6*, and SSC marker gene *Ret*, along with phospho-ERK1/2, decreased in cultured SSCs after RA treatment, while *Stra8* transcript levels increased (Figure 3A and B; Supplementary Figure 2). To explore whether ERK activity changes during early spermatogonial differentiation, we developed a lentiviral differentiation reporter in ERK-KTR SSCs using a *Stra8* promoter fragment (Figure 3C) [69]. Reporter expression was barely detectable in the absence of RA but increased up to 4 days following treatment (Figure 3D and E). Whereas ERK activity was negatively associated with expression of the differentiation reporter prior to treatment, this correlation was lost after 3 days of exposure (Figure 3F and G). Average ERK activity was decreased in the presence or absence of RA, and we observed a shortened pulse period and decreased prominence in differentiating cells (Figure 3H). These data indicate that the dynamic pattern of the ERK signal is altered during in vitro differentiation, concurrent with reduced expression of NFRs.

Spry4 functions as a negative feedback regulator downstream of the RAS/RAF/MEK/ERK cascade

Spry family members have cell type-specific effects on signaling, including negative feedback control of the ERK MAPK and PKC pathways [40, 65]. However, the functional significance of *Spry4* in germ cells is unknown. To address this and link *Spry4* specifically to ERK MAPK in SSCs, we first examined the upstream regulation of *Spry4*. At the

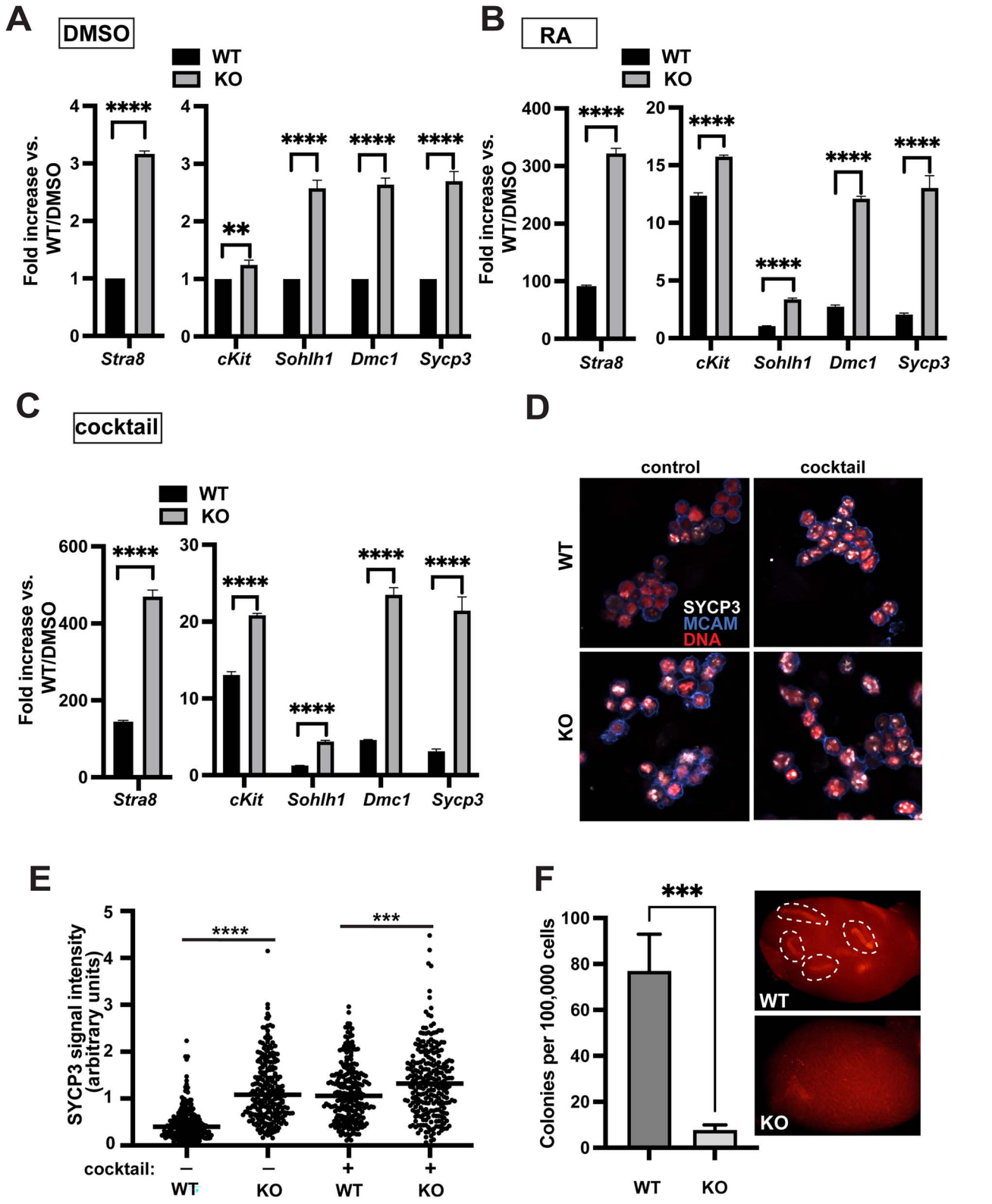

Figure 5. Spry4 loss leads to a differentiated phenotype in vitro. (A–C) qRT-PCR showing upregulation of indicated genes in *Spry4* KO SSCs (displayed as fold-change relative to DMSO-treated scramble control values) following incubation for 2 days with DMSO (A), 1 μM RA (B), or differentiation cocktail (C). One representative experiment shown. Bars denote mean ± SD of technical replicates ($n = 3$ experiments). Unpaired *t*-test on delta CT values: $^{**}p < 0.01$, $^{****}p < 0.0001$. (D) Immunostaining for anti-SYCP3 (white) and anti-MCAM (blue) in *Spry4* KO or wildtype scramble control SSCs after 3 days of incubation with DMSO or differentiation cocktail. Red = DNA. Scale bar = 20 μM. $N = 3$ experiments. (E) Quantification of nuclear anti-SYCP3 signal using image analysis ($n = 248$ cells/group; unpaired *t*-test: WT control vs. KO control, $p < 0.0005$, WT cocktail vs. KO cocktail, $p < 0.001$, WT control vs. WT cocktail, $p < 0.001$, and KO control vs. KO cocktail, $p < 0.01$). (F) SSC transplantation data for *Spry4* KO or WT control SSCs (left; unpaired *t*-test, $p < 0.0001$, bars denote mean ± SEM; pooled data from 3 experiments). Fluorescent stereomicrographs of representative whole-mount testes are shown on the right, with selected colonies encircled (dashed lines) in the WT (top) and none visible in the KO (bottom).

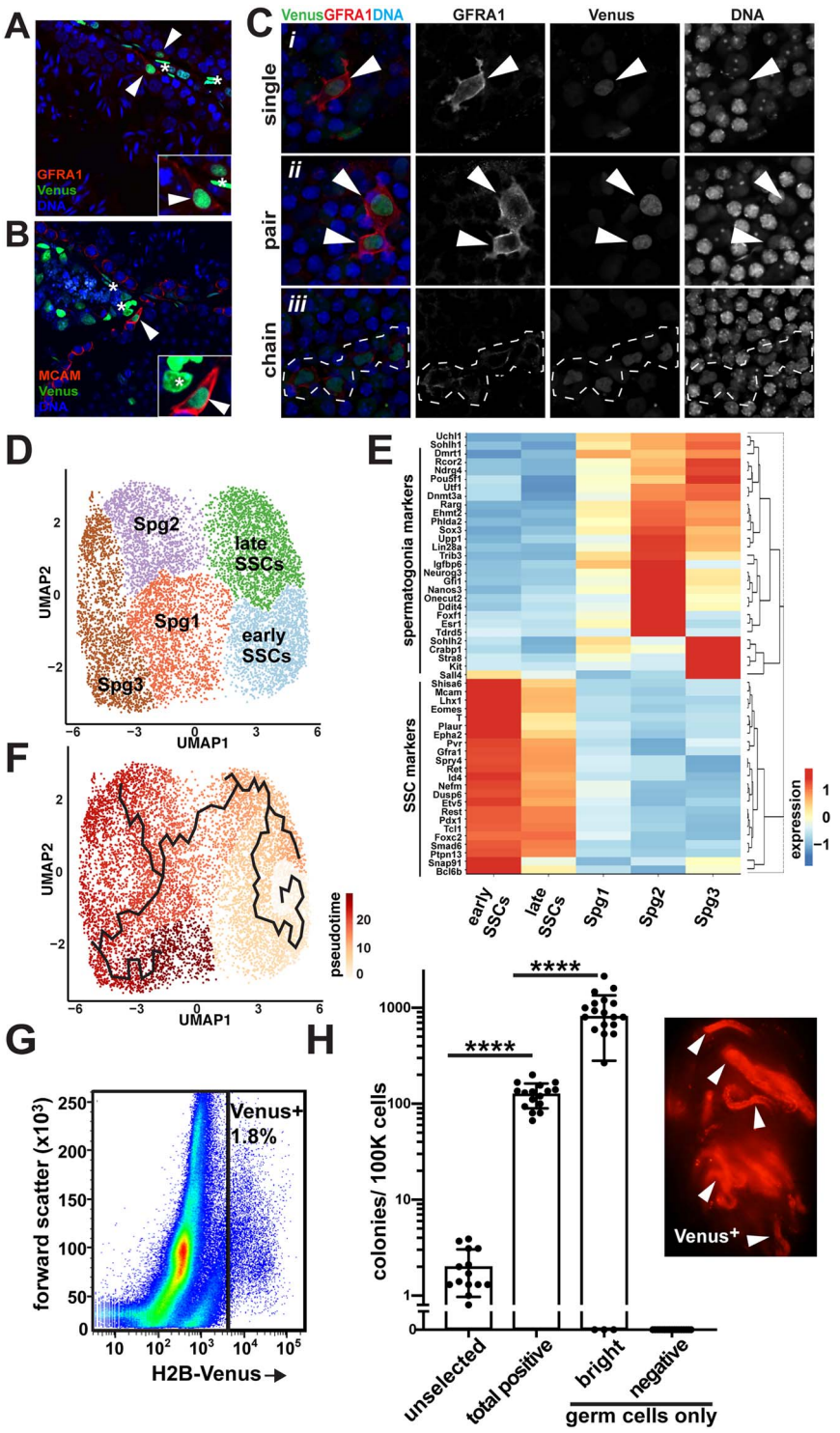

Figure 6. *Spry4* promoter activity marks adult SSCs. (A, B) Adult *Spry4*$^{H2B\text{-}Venus}$ testis cryosections were stained with (A) anti-GFRA1 (red) or (B) anti-MCAM (red). Venus fluorescence is false-colored green. Arrowheads = Spg_{undiff} (enlarged in insets). Asterisks = *Spry4*$^{H2B\text{-}Venus}$-positive somatic cells in the interstitial space. (C) Whole-mount immunostaining of *Spry4*$^{H2B\text{-}Venus}$ tubules for GFRA1, depicting a singlet (i), a pair (ii), and a chain of four (iii, dashed outline). Very faint *Spry4*$^{H2B\text{-}Venus}$ is visible in Sertoli nuclei, identifiable by distinctive nuclear morphology and DAPI-intense satellite karyosomes. (D) UMAP clustering from scRNA-seq analysis of sorted Venus-positive Spg_{undiff} following regression-out of the cell cycle signature (pooled, sorted cells from 3 tamoxifen-induced GCRT;Venus mice). (E) Heatmap clustered by gene, showing scaled gene expression for each annotated UMAP cluster. (F) UMAP clustering based on pseudotime analysis. (G, H) *Spry4*$^{H2B\text{-}Venus}$ mice were crossed with ubiquitous Tomato mice (to obtain Tomato^{+} testicular cells) or GCRT mice (to obtain exclusively Tomato^{+} germ cells after tamoxifen induction). (G) Representative scatterplot showing gating of Venus+ fraction of FACS-sorted testicular cells from *Spry4*$^{H2B\text{-}Venus}$;*tdTomato* mice. (H) Left: transplantation assay showing log-scale increase in SSC activity in the total Venus^{+} cell fraction ($n = 16$ testes) vs. the sorted, ungated control ("unselected"; from Tomato mice; $n = 14$) and in Venus-bright ($n = 21$) vs. Venus-negative ($n = 17$) germ cells from GCRT; Spry4$^{H2B\text{-}Venus}$ mice (unpaired *t*-test: ****$p < 0.0001$; pooled data from 3 experiments for [Venus-bright vs. -negative] and 2 experiments [for Venus+ vs. unselected]). Right: representative whole-mount recipient testis from Venus+ group (arrowheads = colonies; red = tdTomato).

transcriptional level, induction of *Spry4* by FGF2 or GDNF was completely abrogated by a chemical inhibitor of MEK1/2 but not by inhibitors of other canonical pathways (i.e., PI3K, PKC, p38 MAPK, or JNK MAPK), indicating relative specificity for the ERK MAPK pathway (Figure 4A, Supplementary Figure 3). To examine *Spry4* downstream function, we disrupted the *Spry4* coding sequence in ERK-KTR SSCs via CRISPR/Cas9 gene editing, leading to a 4-bp deletion, frameshift, and early stop codon (Figure 4B, inset; Supplementary Figure 4). Compared to non-edited SSC clones, those with *Spry4* loss exhibited increased ERK activity, based on KTR localization, within minutes of exposure to FGF2 (Figure 4B, Supplementary Figure 5). These data suggest that even low, basal levels of SPRY4 (i.e., in starved cells) are sufficient to regulate ERK MAPK. Analysis of dynamic ERK results in Spry4 KO clones vs. wildtype controls did not reveal significant alterations in the patter of pulsatile ERK behavior in the absence of SPRY4 (Supplementary Figure 6). *Spry4* has been reported to suppress ERK signaling through either RAS-dependent or RAS-independent mechanisms depending on cell type [40]. To address this, we detected GTP-RAS using a RAF1 RAS-binding domain (RBD) pull-down assay. We found elevated active RAS in GF-treated cells, which although not statistically significant, trends toward enhancement of RAS activity in cells with reduced *Spry4* and diminution in cells with *Spry4* overexpression (Figure 4C). This was consistent with corresponding immunoblot data demonstrating slightly increased p-ERK in *Spry4*-deficient cells compared to controls or those with constitutive overexpression of *Spry4* (Figure 4D; Supplementary Figure 7). Collectively, these data indicate that *Spry4* is a negative feedback regulator of the ERK MAPK pathway in germ cells.

Spry4 loss leads to a differentiated phenotype in vitro

Since *Spry4* is expressed in a cell population in vivo with the potential to self-renew and regulates ERK MAPK, which has been linked to SSC self-renewal, we next studied the phenotypic consequences of *Spry4* depletion. Cells were cultured in growth medium with DMSO or RA or in an RA-containing medium formulation with additional cytokines (i.e., Kit ligand and NRG1) designed to enhance differentiation (Supplementary Figure 8A). Compared to wildtype controls, cells lacking *Spry4* exhibited increased expression of a panel of differentiation markers (*Stra8*, *Kit*, *Sohlh1*, *Dmc1*, and *Sycp3*) in all conditions (Figure 5A–C). Consistent with this, *Spry4* KO cells exhibited increased protein expression for SYCP3, which was most apparent in growth medium (Figure 5D–E). No consistent effects were seen on expression of SSC markers *Gfra1* and *Id4* (Supplementary Figure 8B). Finally, transplantation analysis revealed decreased stem cell activity in *Spry4* KO cultures compared to WT controls (Figure 5F). To address whether the regenerative capacity of SSCs depends on *Spry4* in vivo, we crossed GCRT mice with mice bearing conditional *Spry4* alleles ($Spry4^{flox}$ mice) [73] and induced recombination with tamoxifen. Following transplantation of total testicular cells and enumeration of tdTomato+ colonies in recipient animals, we found no difference in stem cell activity between *GCRT*;$Spry4^{+/+}$ controls or *GCRT*;$Spry4^{flox/flox}$ cells (Supplementary Figure 9). Taken together, these data suggest that the effect of *Spry4* loss is apparent in vitro but not in vivo.

Spry4 promoter activity marks adult SSCs

To visualize *Spry4*-expressing cells in situ, a nuclear-localized *Spry4* reporter was recently developed, in which an H2B-linked Venus fluorophore fusion protein cDNA was knocked into the endogenous *Spry4* locus (referred to as $Spry4^{H2B\text{-}Venus}$), comprising a highly sensitive, FGF-responsive, transcriptional read-out of *Spry4* promoter activity [46]. To determine whether $Spry4^{H2B\text{-}Venus}$ expression marks phenotypic SSC-like cells, we performed immunostaining on adult $Spry4^{H2B\text{-}Venus}$ testis tissue to detect GFRA1 or MCAM protein, respectively (Figure 6A and B). $Spry4^{H2B\text{-}Venus}$ was co-expressed with $GFRA1^+$ and was also found in MCAM-bright cells, whereas $Spry4^{H2B\text{-}Venus}$ was undetectable in other germ cells. In order to quantify the extent to which the GFRA1 immuno-positive population overlaps with the $Venus^+$ germ cell population, we scored intratubular cells as positive or negative for GFRA1, Venus, and DAZL (as a germ cell marker), using imaging by confocal microscopy (Supplementary Figure 10). This revealed that the $GFRA1^+$ and $Venus^+$ germ cell pools were substantially but not completely overlapping, with $79 \pm 2\%$ of $GFRA1^+$ cells positive for Venus and $95 \pm 5\%$ of $Venus^+$ cells positive for GFRA1. We then performed whole-mount immunostaining for $GFRA1^+$ and confirmed that $Spry4^{H2B\text{-}Venus}$ is expressed not only in A_{pair} and $A_{aligned}$ undifferentiated spermatogonia but also in A_{single} spermatogonia, considered to be the primary SSC cell-containing population (Figure 6C). Of note, most of the $Venus^+$ population in the testis comprised a wide variety of somatic cell types (e.g., putative peritubular, Leydig, endothelial, and Sertoli cells) that expressed bright or faint $Spry4^{H2B\text{-}Venus}$ (Figure 6A–C, Supplementary Figure 10).

We also explored the expression profiles of Venus-positive germ cells. To this end, we bred *Gfra1-CreER*^{T2};*Rosa26-LSL-tdTomato*;$Spry4^{H2B\text{-}Venus}$ mice (referred to as GCRT;Venus mice) in which Spg_{undiff} (but not somatic cells) exhibit tdTomato expression after tamoxifen induction. Sorted tdTomato-positive/Venus-positive germ cells were subject to single-cell RNA sequencing (10x Genomics platform). As expected, this strategy yielded an extremely pure population of spermatogonia (98.2% [9265/9431 cells]). Small numbers of presumptive contaminants were also found, including later-stage germ cells (1.6%; spermatocytes and spermatids), as well as (<0.2%) of somatic cells (endothelial and hematopoietic cells). Non-spermatogonia were excluded from subsequent analyses. Upon initial clustering using UMAP, five major populations could be defined, spanning from early SSC-like cells to early Spg_{undiff} (Supplementary Figure 11A). However, initial examination of the gene expression profiles of these clusters suggested that a portion of the SSC-like population was co-mingled with cells with more differentiated features. We hypothesized that such conflation of populations was due to a strong shared signature of mitotic activity. On this basis, we analyzed the data after regressing out the cell cycle signature (Figure 6D) [74]. The regressed UMAP clusters closely aligned with expected expression profiles for SSCs (two clusters with the highest levels of canonical stem cell marker genes and absent or low expression of progenitor or Spg_{undiff} markers) vs. spermatogonia (three clusters with lower SSC markers and robust Spg_{undiff} markers; Figure 6D and E). We superimposed the initial (i.e., non-regressed) cluster color coding upon the cell cycle-regressed UMAP clusters; this confirmed that the cell cycle signature hindered separation of mitotic SSCs from spermatogonia

(Supplementary Figure 11B). Using the cell cycle-regressed data going forward, we designated the two clusters of SSC-like cells as "early SSCs" (highest levels of SSC markers, e.g. *Id4*, *Pdx1*, *Eomes*, *T*, and *Gfra1*) and "late SSCs" (lower levels of SSC markers; Figure 6D; Supplementary Figure 12A). Among the remaining clusters of spermatogonia, all exhibiting low expression of SSC markers, we designated these three as "Spg1," "Spg2," and "Spg3," based on increasing levels of mRNA corresponding to late Spg_{undiff} markers (e.g., *Kit* and *Stra8*; Supplementary Figure 12B). As expected from our data on $MCAM^+$ germ cells (see Figure 1H), early SSCs exhibited the most robust expression of *Spry4* and *Dusp6*. We then visualized the data based on pseudotime analysis and confirmed that the early SSC cluster represented the most primitive population (Figure 6F). Color coding of these clusters according to cell cycle signature revealed that a subset of SSCs and of spermatogonia, especially Spg1 and Spg3, were enriched for hallmarks of proliferation, while Spg2 appeared notably quiescent and also exhibited the greatest expression of *Sox3* and *Neurog3*, suggestive of distinct early committed progenitor population (Supplementary Figure 12B and C) [1, 75]. Spg3 cells were notable for the highest levels of later differentiation markers *Kit* and *Stra8*. Gene set enrichment analysis comparing the two combined SSC and three combined spermatogonia clusters revealed enrichment for "KRAS signaling up" (NES 1.57, nominal $p = 0$, FDR q-val = 0.034), consistent with the significance of growth factor/RAS pathway signaling in SSCs (Supplementary Figure 12D) [76, 77]. In addition, a substantial number of differentially expressed genes was identified, whose functions in SSCs remain obscure (Supplementary Figure 12E). Concordant with our expression data above (see Figure 1H), *Spry4* expression progressively decreased from early SSCs to Spg3 (Supplementary Figure 12F). Taken together, these data indicate that strong *Spry4* promoter activity marks phenotypic adult SSCs in vivo.

To determine whether $Spry4^{H2B\text{-}Venus}$ marks functional adult stem cells in vivo, we performed SSC transplantation using selected cells from offspring from two different types of mouse crosses. First, $Spry4^{H2B\text{-}Venus}$*;tdTomato* animals were generated by breeding, as a source of cells that ubiquitously express tdTomato, for the purpose of visualizing transplanted colonies derived from unselected vs. total $Venus^+$ testicular cell pools (Figure 6G). Second, we used GCRT;Venus mice described above, in which Spg_{undiff} exclusively exhibit *tdTomato* expression at early time points (i.e., days 9–10) after tamoxifen induction. Using these two different sets of donors, singlet, freshly dissociated adult $tdTomato^+$ testicular cells were flow-sorted into four groups: (i) the parental cell pool from $Spry4^{H2B\text{-}Venus}$*;tdTomato* mice (referred to as "unselected"), (ii) the $Venus^+$ subpopulation from $Spry4^{H2B\text{-}Venus}$*;tdTomato* mice, (iii) Venus-bright Spg_{undiff} from induced GCRT;Venus mice, and (iv) Venus-negative germ cells from induced GCRT;Venus mice. Following transplantation into busulfan-treated recipients, $tdTomato^+$ colonies were counted 2 months later, revealing that $Venus^+$ total testicular cells were ~60-fold enriched for SSC activity (Figure 6H). As expected, the unselected control cells yielded ~2.0 colonies (95% CI: 1.4–2.6) per 100 000 cells, similar to historical controls [78]. Moreover, the highest stem cell activity was observed using Venus-bright Spg_{undiff}, yielding an average of 814 colonies (95% CI: 571–1058) per 100 000 cells. Stem cell activity in the Venus-negative Spg_{undiff} group was below the detection limit, despite transplantation of a ~5-fold excess of cells compared to the Venus-bright Spg_{undiff} group. These data indicate that the vast majority of stem cell activity was contained within the Venus-bright Spg_{undiff} population. Assuming ~5–10% transplantation efficiency [78–80], the data suggest that ~8–16% of Venus-bright adult germ cells in vivo function as SSCs in this assay. Taken together, the transplantation and scRNA sequencing data indicate that strong *Spry4* promoter activity marks adult SSCs in vivo.

Discussion

The faithful integration of different extracellular cues depends upon myriad intracellular regulatory mechanisms, acting at various nodes in a given pathway. Here, we identified a *Spry4*-driven negative feedback mechanism that controls the signaling output from GF-dependent receptor tyrosine kinases in SSCs. *Spry4* was selectively induced in vitro by GFs that support self-renewal (i.e., FGF2 and GDNF). Interrogation of $MCAM^+$ germ cells revealed that robust expression of negative feedback regulators of ERK MAPK signaling is a unique feature of Spg_{undiff} in vivo. Functionally, ERK MAPK signaling induced *Spry4* expression, leading to suppression of the pathway, in part, through effects on RAS activity. Cultured SSCs exhibited pulsatile ERK responses to GFs and a negative correlation of ERK activity with increasing differentiation status. Through gene expression profiling and transplantation of germ cells expressing a $Spry4^{H2B\text{-}Venus}$ reporter, we found that *Spry4* expression effectively delineates SSCs in vivo. Normal *Spry4* function was critical for SSC maintenance in vitro since *Spry4* loss caused upregulation of differentiation markers and loss of stem cell activity.

While previous lines of evidence indicated that cell-autonomous regulation of GF-mediated signaling is critical for maintaining homeostasis of spermatogonia and can be achieved in part through robust intracellular negative feedback control [15, 35, 36, 81], the significance of Spry family genes in SSCs has been unclear. Our results support *Spry4* as a marker for adult SSCs in vivo, but cultured SSCs were uniquely dependent on *Spry4* for ERK MAPK negative feedback in order to maintain stem cell activity. The latter result contrasts to SSCs in vivo that can apparently withstand *Spry4* loss based on transplantation of testicular cells from induced *GCRT;*$Spry4^{flox/flox}$ mice. A potential explanation could be that SSCs in vivo but not cultured SSCs might compensate for *Spry4* loss through upregulation of other Spry family members (i.e., *Spry1* and *Spry2*) or other NFRs such as Dusps. In addition, we speculate that the GF-rich medium required for SSC culture may expose limits to the inherent feedback mechanisms that collectively prevent excessive ERK MAPK activation. Other data from studies that experimentally alter upstream ligand-dependent or ligand-independent ERK MAPK signaling are consistent with the existence of such limits. For example, self-renewal of SSCs in vitro can be abrogated by high doses of FGF [23], which can also enhance the differentiated gene expression program [14, 24]. However, given the technical challenges in measuring both ambient levels of GFs in the niche in vivo and corresponding ERK MAPK activity, it is unclear what comprises the physiologically relevant range of GF concentrations detected by SSCs in situ. Such data would be needed in order to elucidate how GFs control SSC

homeostasis. One study found that SSC gene expression was globally unaltered by reduction in FGF dosage, but expression of the negative feedback regulator *Dusp6* was decreased in GFRA1-expressing cells from *FGF5*$^{-/-}$ animals, suggesting that intracellular ERK MAPK negative feedback might be somewhat alleviated under GF-reduced conditions [21]. A recent study also indicated that the ambient GF environment of homeostatic SSCs is quite constrained but that GF signaling is significantly enhanced during cytotoxic stress-induced regeneration [82].

In our study, we found a strong correlation between *Spry4* expression (either at the mRNA level or using transplantation of germ cells from *Spry4*$^{H2B\text{-}Venus}$ mice) and the SSC phenotype. The *Spry4*$^{H2B\text{-}Venus}$ mouse provides a validated measure of p-ERK [46]. Therefore, our findings lend further credence to the idea that active ERK MAPK signaling is a central feature of the stem cell but not the progenitor population in vivo [14, 24, 83]. While it is possible that transcriptional changes during early differentiation could activate negative feedback genes other than *Spry4* (or *Dusp6*) to undertake analogous functions, we did not find evidence of this in our scRNA-seq data (Supplementary Figure 12F). It should be noted, also, that the SSC population is increasingly thought to comprise cells within multiple potentially inter-convertible states [1, 12–14, 34], yet the relevant time scales for such cell-state transitions are enigmatic. Future studies that integrate gene expression and real-time measurement of signaling could capture these transitions. Our extrapolations indicate that SSCs comprise ∼1–2 in 8 of the Venus-bright germ cells in the adult testis, but a remaining question is whether any substantial amount of stem cell activity resides in the Venus-dim or Venus-negative fractions of germ cells. One caveat, though, is that the transplantation assay itself may reflect a regenerative setting in the mouse testis more than a homeostatic one since committed progenitors may display colonization ability upon transplantation [1].

An emergent feature of *Spry4* function is cell type specificity with respect to upstream ligand/receptor pairs and downstream targets. Consistent with reports in other cell types, we found that *Spry4* is strongly induced by FGF but not EGF, despite the ability of the latter to induce ERK MAPK signaling in SSCs [81]. To our knowledge, *Spry4* has not been previously reported as a GDNF-responsive gene in any cell type. This feature is, however, perhaps unsurprising given the role of *Spry1* in GDNF/Ret signaling [47]. While GDNF and FGF2 both exert strong effects on expression of *Spry4* (and also *Dusp6*), it is also possible that other upstream ligand–receptor interactions could be relevant. Similarly, we speculate that future studies will reveal analogous functions for other GF-dependent negative regulators uniquely in SSCs. In contrast to *Dusp6*, which acts largely on ERK, the detailed mechanisms by which Spry proteins modulate the pathway in different cell types remain unclear [65]. Spry proteins exert repressive actions by targeting various nodes, and their inhibitory interactions occur downstream of RTKs but upstream of ERK, including with GRB2, RAF1, DYRK1A, and other effectors [40, 84–86]. SPRY4 itself is reported to interact directly with RAF1 and TESK1 [40, 87]. While our data demonstrate that SPRY4 in SSCs acts at or above the level of RAS, further experiments will be required to demonstrate the specific binding partners and rule out the possibility of additional downstream interactions.

Despite the fact that ERK MAPK supports SSC self-renewal, our data imply that pathway activity must be maintained within a narrow range in vitro to prevent precocious differentiation. This concept is reminiscent of prior results showing that hyperactivation of mTORC1 downstream of GFs in *Zbtb16/Plzf*- or *Tsc2*-deficient SSCs leads to loss of self-renewal and precocious differentiation through a negative feedback mechanism [81, 88]. An analogous paradigm exists in tumor models in which subtle variations in MAPK signaling determine cell fate outcome, such as transformation vs. cellular toxicity [89, 90] or proliferation vs. differentiation [91]. Such dichotomous cell fates, dependent on intrinsic negative feedback, may extend to other ERK MAPK-dependent pathologies, given that deregulation of this pathway underlies many cancers and developmental diseases. However, our data also present an apparent paradox that relates to a class of paternal age-associated congenital disorders driven by weakly activating mutations in genes upstream of the ERK MAPK pathway. For example, gain-of-function mutations in *FGFR2* drive self-selection of SSC clones during aging through mild hyperactivation of ERK MAPK [61, 92]. Evidently, the presence of endogenous negative feedback regulators in SSCs, such as *Spry4* and *Dusp6*, cannot fully mitigate such phenotypes in the human testis associated with GF-driven selfish selection. This is surprising, given the relatively modest magnitude of pathway activation thought to be conferred by point mutations that drive paternal age-associated congenital disorders compared to oncogenic mutations [93]. Furthermore, even strong-acting somatic cancer mutations in GF receptor components can elicit sufficient negative feedback in tumor cells to suppress downstream signaling [94]. Further investigation will be required to understand this paradox and whether it could be related to species-specific differences.

In conclusion, we show here that a *Spry4*-mediated negative feedback loop fine-tunes the response to niche-derived self-renewal factors in adult SSCs. While this study focused on *Spry4*, other feedbacks have been identified in different model systems and biological contexts that function to limit ERK MAPK activity. These include not only genes that are transcriptionally upregulated by ERK MAPK (e.g., *Dusp6*) but also cross-talk from parallel pathways that may serve to modulate ERK MAPK output. Future studies will need to address the integrated effects of such signals in a holistic fashion, not only to improve techniques for long-term culture of SSCs from humans and other species but also to develop therapeutic strategies to address infertility.

Supplementary material

Supplementary material is available at *BIOLRE* online.

Acknowledgment

We thank Dr. S. Morgani for help with *Spry4*$^{H2B\text{-}Venus}$ mice and Dr. S. Chen for input on the manuscript. We thank the Weill Cornell Flow Cytometry, Genomics Resources, and Optical Microscopy Core Facilities for assistance with experiments. We thank Drs. S. Jain, H. Enomoto, and J. Milbrandt for *Gfra1-CreER*^{T2} mice.

Conflict of Interest: The authors have declared that no conflict of interest exists.

Authors' contributions

YL and LM conceived and designed the study, performed experiments, analyzed data, and wrote the manuscript; MY, TN, HA, OK, PM, MG, and AH performed experiments; HUV, OE, and YH analyzed data; YL, TE, and SR wrote the manuscript; and MS conceived, designed, and supervised the study, performed experiments, analyzed data, and wrote the manuscript.

Data Availability

The data underlying this article are available in the article, in its online supplementary material, and at the following link: https://weillcornellmed.shinyapps.io/Seandel_TNB_cell_cycle/.

References

1. Nakagawa T, Nabeshima Y, Yoshida S. Functional identification of the actual and potential stem cell compartments in mouse spermatogenesis. *Dev Cell* 2007; **12**:195–206.
2. Lin B, Coleman JH, Peterson JN, Zunitch MJ, Jang W, Herrick DB, Schwob JE. Injury induces endogenous reprogramming and dedifferentiation of neuronal progenitors to multipotency. *Cell Stem Cell* 2017; **21**:761–774.e5.
3. Rompolas P, Mesa KR, Greco V. Spatial organization within a niche as a determinant of stem-cell fate. *Nature* 2013; **502**: 513–518.
4. Buganim Y, Faddah DA, Cheng AW, Itskovich E, Markoulaki S, Ganz K, Klemm SL, van Oudenaarden A, Jaenisch R. Single-cell expression analyses during cellular reprogramming reveal an early stochastic and a late hierarchic phase. *Cell* 2012; **150**:1209–1222.
5. Tata PR, Mou H, Pardo-Saganta A, Zhao R, Prabhu M, Law BM, Vinarsky V, Cho JL, Breton S, Sahay A, Medoff BD, Rajagopal J. Dedifferentiation of committed epithelial cells into stem cells in vivo. *Nature* 2013; **503**:218–223.
6. Chakkalakal JV, Jones KM, Basson MA, Brack AS. The aged niche disrupts muscle stem cell quiescence. *Nature* 2012; **490**:355–360.
7. Bernet JD, Doles JD, Hall JK, Kelly Tanaka K, Carter TA, Olwin BB. p38 MAPK signaling underlies a cell-autonomous loss of stem cell self-renewal in skeletal muscle of aged mice. *Nat Med* 2014; **20**:265–271.
8. Villeda SA, Luo J, Mosher KI, Zou B, Britschgi M, Bieri G, Stan TM, Fainberg N, Ding Z, Eggel A, Lucin KM, Czirr E, *et al.* The ageing systemic milieu negatively regulates neurogenesis and cognitive function. *Nature* 2011; **477**:90–94.
9. Meng X, Lindahl M, Hyvönen ME, Parvinen M, de Rooij DG, Hess MW, Raatikainen-Ahokas A, Sainio K, Rauvala H, Lakso M, Pichel JG, Westphal H, *et al.* Regulation of cell fate decision of undifferentiated spermatogonia by GDNF. *Science* 2000; **287**: 1489–1493.
10. Kubota H, Avarbock MR, Brinster RL. Growth factors essential for self-renewal and expansion of mouse spermatogonial stem cells. *Proc Natl Acad Sci U S A* 2004; **101**:16489–16494.
11. Oatley JM, Avarbock MR, Telaranta AI, Fearon DT, Brinster RL. Identifying genes important for spermatogonial stem cell self-renewal and survival. *Proc Natl Acad Sci U S A* 2006; **103**: 9524–9529.
12. Hara K, Nakagawa T, Enomoto H, Suzuki M, Yamamoto M, Simons BD, Yoshida S. Mouse spermatogenic stem cells continually interconvert between equipotent singly isolated and syncytial states. *Cell Stem Cell* 2014; **14**:658–672.
13. Nakagawa T, Sharma M, Nabeshima YI, Braun RE, Yoshida S. Functional hierarchy and reversibility within the murine spermatogenic stem cell compartment. *Science* 2010; **328**:62–67.
14. La HM, Mäkelä JA, Chan AL, Rossello FJ, Nefzger CM, Legrand JMD, De Seram M, Polo JM, Hobbs RM. Identification of dynamic undifferentiated cell states within the male germline. *Nat Commun* 2018; **9**:2819.
15. Tokue M, Ikami K, Mizuno S, Takagi C, Miyagi A, Takada R, Noda C, Kitadate Y, Hara K, Mizuguchi H, Sato T, Taketo MM, *et al.* SHISA6 confers resistance to differentiation-promoting Wnt/beta-catenin signaling in mouse spermatogenic stem cells. *Stem Cell Reports* 2017; **8**:561–575.
16. Oatley JM, Brinster RL. Regulation of spermatogonial stem cell self-renewal in mammals. *Annu Rev Cell Dev Biol* 2008; **24**: 263–286.
17. Parker N, Falk H, Singh D, Fidaleo A, Smith B, Lopez MS, Shokat KM, Wright WW. Responses to glial cell line-derived neurotrophic factor change in mice as spermatogonial stem cells form progenitor spermatogonia which replicate and give rise to more differentiated progeny. *Biol Reprod* 2014; **91**:92.
18. Sharma M, Braun RE. Cyclical expression of GDNF is required for spermatogonial stem cell homeostasis. *Development* 2018; **145**(5):dev151555.
19. Oatley JM, Avarbock MR, Brinster RL. Glial cell line-derived neurotrophic factor regulation of genes essential for self-renewal of mouse spermatogonial stem cells is dependent on Src family kinase signaling. *J Biol Chem* 2007; **282**:25842–25851.
20. Ishii K, Kanatsu-Shinohara M, Toyokuni S, Shinohara T. FGF2 mediates mouse spermatogonial stem cell self-renewal via upregulation of Etv5 and Bcl6b through MAP2K1 activation. *Development* 2012; **139**:1734–1743.
21. Kitadate Y, Jörg DJ, Tokue M, Maruyama A, Ichikawa R, Tsuchiya S, Segi-Nishida E, Nakagawa T, Uchida A, Kimura-Yoshida C, Mizuno S, Sugiyama F, *et al.* Competition for mitogens regulates spermatogenic stem cell homeostasis in an open niche. *Cell Stem Cell* 2019; **24**:79–92.e6.
22. Zhang Y, Wang S, Wang X, Liao S, Wu Y, Han C. Endogenously produced FGF2 is essential for the survival and proliferation of cultured mouse spermatogonial stem cells. *Cell Res* 2012; **22**: 773–776.
23. Kubota H, Avarbock MR, Brinster RL. Culture conditions and single growth factors affect fate determination of mouse spermatogonial stem cells. *Biol Reprod* 2004; **71**:722–731.
24. Takashima S, Kanatsu-Shinohara M, Tanaka T, Morimoto H, Inoue K, Ogonuki N, Jijiwa M, Takahashi M, Ogura A, Shinohara T. Functional differences between GDNF-dependent and FGF2-dependent mouse spermatogonial stem cell self-renewal. *Stem Cell Reports* 2015; **4**:489–502.
25. Shea KL, Xiang W, LaPorta VS, Licht JD, Keller C, Basson MA, Brack AS. Sprouty1 regulates reversible quiescence of a self-renewing adult muscle stem cell pool during regeneration. *Cell Stem Cell* 2010; **6**:117–129.
26. Mishra A, Oulès B, Pisco AO, Ly T, Liakath-Ali K, Walko G, Viswanathan P, Tihy M, Nijjher J, Dunn SJ, Lamond AI, Watt FM. A protein phosphatase network controls the temporal and spatial dynamics of differentiation commitment in human epidermis. *Elife* 2017; **6**:e27356.
27. Baumgartner C, Toifl S, Farlik M, Halbritter F, Scheicher R, Fischer I, Sexl V, Bock C, Baccarini M. An ERK-dependent feedback mechanism prevents hematopoietic stem cell exhaustion. *Cell Stem Cell* 2018; **22**:879–892.e6.
28. Hiratsuka T, Bordeu I, Pruessner G, Watt FM. Regulation of ERK basal and pulsatile activity control proliferation and exit from the stem cell compartment in mammalian epidermis. *Proc Natl Acad Sci U S A* 2020; **117**:17796–17807.
29. Hamra FK, Schultz N, Chapman KM, Grellhesl DM, Cronkhite JT, Hammer RE, Garbers DL. Defining the spermatogonial stem cell. *DevBiol* 2004; **269**:393–410.
30. Terry NA, Tulina N, Matunis E, DiNardo S. Novel regulators revealed by profiling drosophila testis stem cells within their niche. *Dev Biol* 2006; **294**:246–257.
31. Liao J, Ng SH, Luk ACS, Suen AHC, Qian Y, Tu J, Fung JCL, Tang NLS, Feng B, Chan WY, Fouchet P, Lee TL. Revealing cellular and molecular transitions in neonatal germ cell differentiation using single cell RNA sequencing. *Development* 2019; **146**: dev174953.

32. Guo J, Grow EJ, Mlcochova H, Maher GJ, Lindskog C, Nie X, Guo Y, Takei Y, Yun J, Cai L, Kim R, Carrell DT, *et al*. The adult human testis transcriptional cell atlas. *Cell Res* 2018; **28**:1141–1157.
33. Prokai D, Pudasaini A, Kanchwala M, Moehlman AT, Waits AE, Chapman KM, Chaudhary J, Acevedo J, Keller P, Chao X, Carr BR, Hamra FK. Spermatogonial gene networks selectively couple to glutathione and pentose phosphate metabolism but not cysteine biosynthesis. *iScience* 2021; **24**:101880.
34. Suzuki S, McCarrey JR, Hermann BP. An mTORC1-dependent switch orchestrates the transition between mouse spermatogonial stem cells and clones of progenitor spermatogonia. *Cell Rep* 2021; **34**:108752.
35. Chan AL, la HM, Legrand JMD, Mäkelä JA, Eichenlaub M, de Seram M, Ramialison M, Hobbs RM. Germline stem cell activity is sustained by SALL4-dependent silencing of distinct tumor suppressor genes. *Stem Cell Reports* 2017; **9**:956–971.
36. La HM, Chan A-L, Legrand JMD, Rossello FJ, Gangemi CG, Papa A, Cheng Q, Morand EF, Hobbs RM. GILZ-dependent modulation of mTORC1 regulates spermatogonial maintenance. *Development* 2018; **145**:dev165324.
37. Hacohen N, Kramer S, Sutherland D, Hiromi Y, Krasnow MA. Sprouty encodes a novel antagonist of FGF signaling that patterns apical branching of the Drosophila airways. *Cell* 1998; **92**: 253–263.
38. Kim HJ, Bar-Sagi D. Modulation of signalling by Sprouty: a developing story. *Nat Rev Mol Cell Biol* 2004; **5**:441–450.
39. Ozaki K, Miyazaki S, Tanimura S, Kohno M. Efficient suppression of FGF-2-induced ERK activation by the cooperative interaction among mammalian Sprouty isoforms. *J Cell Sci* 2005; **118**: 5861–5871.
40. Sasaki A, Taketomi T, Kato R, Saeki K, Nonami A, Sasaki M, Kuriyama M, Saito N, Shibuya M, Yoshimura A. Mammalian Sprouty 4 suppresses Ras-independent ERK activation by binding to Raf 1. *Nat Cell Biol* 2003; **5**:427–432.
41. Sasaki A, Taketomi T, Wakioka T, Kato R, Yoshimura A. Identification of a dominant negative mutant of Sprouty that potentiates fibroblast growth factor- but not epidermal growth factor-induced ERK activation. *J Biol Chem* 2001; **276**:36804–36808.
42. Alsina FC, Irala D, Fontanet PA, Hita FJ, Ledda F, Paratcha G. Sprouty 4 is an endogenous negative modulator of Trk a signaling and neuronal differentiation induced by NGF. *PloS One* 2012; **7**:e32087.
43. Keefe Davis T, Hoshi M, Jain S. Stage specific requirement of Gfralpha1 in the ureteric epithelium during kidney development. *Mech Dev* 2013; **130**:506–518.
44. Madisen L, Zwingman TA, Sunkin SM, Oh SW, Zariwala HA, Gu H, Ng LL, Palmiter RD, Hawrylycz MJ, Jones AR, Lein ES, Zeng H. A robust and high-throughput Cre reporting and characterization system for the whole mouse brain. *Nat Neurosci* 2010; **13**:133–140.
45. Simon CS, Rahman S, Raina D, Schröter C, Hadjantonakis AK. Live visualization of ERK activity in the mouse blastocyst reveals lineage-specific Signaling dynamics. *Dev Cell* 2020; **55**:341–353.e5.
46. Morgani SM, Saiz N, Garg V, Raina D, Simon CS, Kang M, Arias AM, Nichols J, Schröter C, Hadjantonakis AK. A Sprouty4 reporter to monitor FGF/ERK signaling activity in ESCs and mice. *Dev Biol* 2018; **441**:104–126.
47. Basson MA, Akbulut S, Watson-Johnson J, Simon R, Carroll TJ, Shakya R, Gross I, Martin GR, Lufkin T, McMahon AP, Wilson PD, Costantini FD, *et al*. Sprouty1 is a critical regulator of GDNF/RET-mediated kidney induction. *Dev Cell* 2005; **8**: 229–239.
48. Martin LA, Seandel M. Serial enrichment of spermatogonial stem and progenitor cells (SSCs) in culture for derivation of long-term adult mouse SSC lines. *J Vis Exp* 2013; **72**:e50017.
49. Kim J, Seandel M, Falciatori I, Wen D, Rafii S. CD34+ testicular stromal cells support long-term expansion of embryonic and adult stem and progenitor cells. *Stem Cells* 2008; **26**:2516–2522.
50. Zhang X, Gunewardena S, Wang N. Nutrient restriction synergizes with retinoic acid to induce mammalian meiotic initiation in vitro. *Nat Commun* 2021; **12**:1758.
51. N'Tumba-Byn T, Yamada M, Seandel M. Loss of tyrosine kinase receptor Ephb2 impairs proliferation and stem cell activity of spermatogonia in culturedagger. *Biol Reprod* 2020; **102**: 950–962.
52. Garbuzov A, Pech MF, Hasegawa K, Sukhwani M, Zhang RJ, Orwig KE, Artandi SE. Purification of GFRalpha1+ and GFRalpha1− spermatogonial stem cells reveals a niche-dependent mechanism for fate determination. *Stem Cell Reports* 2018; **10**: 553–567.
53. Kanatsu-Shinohara M, Morimoto H, Shinohara T. Enrichment of mouse spermatogonial stem cells by melanoma cell adhesion molecule expression. *Biol Reprod* 2012; **87**:139.
54. Seandel M, James D, Shmelkov SV, Falciatori I, Kim J, Chavala S, Scherr DS, Zhang F, Torres R, Gale NW, Yancopoulos GD, Murphy A, *et al*. Generation of functional multipotent adult stem cells from GPR125+ germline progenitors. *Nature* 2007; **449**: 346–350.
55. Yamada M, Cai W, Martin LA, N'Tumba-Byn T, Seandel M. Functional robustness of adult spermatogonial stem cells after induction of hyperactive Hras. *PLoS Genet* 2019; **15**:e1008139.
56. Stuart T, Butler A, Hoffman P, Hafemeister C, Papalexi E, Mauck WM III, Hao Y, Stoeckius M, Smibert P, Satija R. Comprehensive integration of single-cell data. *Cell* 2019; **177**:1888–1902.e21.
57. McCarthy DJ, Campbell KR, Lun ATL, Wills QF. Scater: pre-processing, quality control, normalization and visualization of single-cell RNA-seq data in R. *Bioinformatics* 2017; **33**: 1179–1186.
58. Aran D, Looney AP, Liu L, Wu E, Fong V, Hsu A, Chak S, Naikawadi RP, Wolters PJ, Abate AR, Butte AJ, Bhattacharya M. Reference-based analysis of lung single-cell sequencing reveals a transitional profibrotic macrophage. *Nat Immunol* 2019; **20**: 163–172.
59. Grive KJ, Hu Y, Shu E, Grimson A, Elemento O, Grenier JK, Cohen PE. Dynamic transcriptome profiles within spermatogonial and spermatocyte populations during postnatal testis maturation revealed by single-cell sequencing. *PLoS Genet* 2019; **15**:e1007810.
60. Qiu X, Hill A, Packer J, Lin D, Ma YA, Trapnell C. Single-cell mRNA quantification and differential analysis with census. *Nat Methods* 2017; **14**:309–315.
61. Martin LA, Assif N, Gilbert M, Wijewarnasuriya D, Seandel M. Enhanced fitness of adult spermatogonial stem cells bearing a paternal age-associated FGFR2 mutation. *Stem Cell Reports* 2014; **3**:219–226.
62. Nagano MC, Yeh JR. The identity and fate decision control of spermatogonial stem cells: where is the point of no return? *Curr Top Dev Biol* 2013; **102**:61–95.
63. Amit I, Citri A, Shay T, Lu Y, Katz M, Zhang F, Tarcic G, Siwak D, Lahad J, Jacob-Hirsch J, Amariglio N, Vaisman N, *et al*. A module of negative feedback regulators defines growth factor signaling. *Nat Genet* 2007; **39**:503–512.
64. Liu Y, Giannopoulou EG, Wen D, Falciatori I, Elemento O, Allis CD, Rafii S, Seandel M. Epigenetic profiles signify cell fate plasticity in unipotent spermatogonial stem and progenitor cells. *Nat Commun* 2016; **7**:11275.
65. Neben CL, Lo M, Jura N, Klein OD. Feedback regulation of RTK signaling in development. *Dev Biol* 2017; **447**:71–89.
66. Mason JM, Morrison DJ, Albert Basson M, Licht JD. Sprouty proteins: multifaceted negative-feedback regulators of receptor tyrosine kinase signaling. *Trends Cell Biol* 2006; **16**:45–54.
67. Regot S, Hughey JJ, Bajar BT, Carrasco S, Covert MW. High-sensitivity measurements of multiple kinase activities in live single cells. *Cell* 2014; **157**:1724–1734.
68. Albeck JG, Mills GB, Brugge JS. Frequency-modulated pulses of ERK activity transmit quantitative proliferation signals. *Mol Cell* 2013; **49**:249–261.

69. Dann CT, Alvarado AL, Molyneux LA, Denard BS, Garbers DL, Porteus MH. Spermatogonial stem cell self-renewal requires OCT4, a factor downregulated during retinoic acid-induced differentiation. *Stem Cells* 2008; **26**:2928–2937.
70. Wang S, Wang X, Ma L, Lin X, Zhang D, Li Z, Wu Y, Zheng C, Feng X, Liao S, Feng Y, Chen J, *et al.* Retinoic acid is sufficient for the in vitro induction of mouse spermatocytes. *Stem Cell Reports* 2016; **7**:80–94.
71. Johnson TA, Niedenberger BA, Kirsanov O, Harrington EV, Malachowski T, Geyer CB. Differential responsiveness of spermatogonia to retinoic acid dictates precocious differentiation but not meiotic entry during steady-state spermatogenesis. *Biol Reprod* 2023; **108**:822–836.
72. Endo T, Romer KA, Anderson EL, Baltus AE, de Rooij DG, Page DC. Periodic retinoic acid-STRA8 signaling intersects with periodic germ-cell competencies to regulate spermatogenesis. *Proc Natl Acad Sci U S A* 2015; **112**:E2347–E2356.
73. Klein OD, Minowada G, Peterkova R, Kangas A, Yu BD, Lesot H, Peterka M, Jernvall J, Martin GR. Sprouty genes control diastema tooth development via bidirectional antagonism of epithelial-mesenchymal FGF signaling. *Dev Cell* 2006; **11**:181–190.
74. Buettner F, Natarajan KN, Casale FP, Proserpio V, Scialdone A, Theis FJ, Teichmann SA, Marioni JC, Stegle O. Computational analysis of cell-to-cell heterogeneity in single-cell RNA-sequencing data reveals hidden subpopulations of cells. *Nat Biotechnol* 2015; **33**:155–160.
75. McAninch D, Mäkelä JA, la HM, Hughes JN, Lovell-Badge R, Hobbs RM, Thomas PQ. SOX3 promotes generation of committed spermatogonia in postnatal mouse testes. *Sci Rep* 2020; **10**: 6751.
76. Subramanian A, Tamayo P, Mootha VK, Mukherjee S, Ebert BL, Gillette MA, Paulovich A, Pomeroy SL, Golub TR, Lander ES, Mesirov JP. Gene set enrichment analysis: a knowledge-based approach for interpreting genome-wide expression profiles. *Proc Natl Acad Sci U S A* 2005; **102**:15545–15550.
77. Liberzon A, Birger C, Thorvaldsdóttir H, Ghandi M, Mesirov JP, Tamayo P. The molecular signatures database (MSigDB) hallmark gene set collection. *Cell Syst* 2015; **1**:417–425.
78. Nagano M, Avarbock MR, Brinster RL. Pattern and kinetics of mouse donor spermatogonial stem cell colonization in recipient testes. *Biol Reprod* 1999; **60**:1429–1436.
79. Shinohara T, Orwig KE, Avarbock MR, Brinster RL. Remodeling of the postnatal mouse testis is accompanied by dramatic changes in stem cell number and niche accessibility. *Proc Natl Acad Sci U S A* 2001; **98**:6186–6191.
80. Nagano MC. Homing efficiency and proliferation kinetics of male germ line stem cells following transplantation in mice. *Biol Reprod* 2003; **69**:701–707.
81. Hobbs RM, Seandel M, Falciatori I, Rafii S, Pandolfi PP. Plzf regulates germline progenitor self-renewal by opposing mTORC1. *Cell* 2010; **142**:468–479.
82. La HM, Liao J, Legrand JMD, Rossello FJ, Chan A-L, Vaghjiani V, Cain JE, Papa A, Lee TL, Hobbs RM. Distinctive molecular features of regenerative stem cells in the damaged male germline. *Nat Commun* 2022; **13**:2500.
83. Hasegawa K, Namekawa SH, Saga Y. MEK/ERK signaling directly and indirectly contributes to the cyclical self-renewal of spermatogonial stem cells. *Stem Cells* 2013; **31**:2517–2527.
84. Yusoff P, Lao DH, Ong SH, Wong ESM, Lim J, Lo TL, Leong HF, Fong CW, Guy GR. Sprouty2 inhibits the Ras/MAP kinase pathway by inhibiting the activation of Raf. *J Biol Chem* 2002; **277**:3195–3201.
85. Wong ES, Lim J, Low BC, Chen Q, Guy GR. Evidence for direct interaction between Sprouty and Cbl. *J Biol Chem* 2001; **276**: 5866–5875.
86. Lao DH, Chandramouli S, Yusoff P, Fong CW, Saw TY, Tai LP, Yu CY, Leong HF, Guy GR. A Src homology 3-binding sequence on the C terminus of Sprouty2 is necessary for inhibition of the Ras/ERK pathway downstream of fibroblast growth factor receptor stimulation. *J Biol Chem* 2006; **281**:29993–30000.
87. Leeksma OC, van Achterberg TAE, Tsumura Y, Toshima J, Eldering E, Kroes WGM, Mellink C, Spaargaren M, Mizuno K, Pannekoek H, de Vries CJM. Human sprouty 4, a new ras antagonist on 5q31, interacts with the dual specificity kinase TESK1. *Eur J Biochem* 2002; **269**:2546–2556.
88. Hobbs RM, la HM, Mäkelä JA, Kobayashi T, Noda T, Pandolfi PP. Distinct germline progenitor subsets defined through Tsc2-mTORC1 signaling. *EMBO Rep* 2015; **16**:467–480.
89. Nieto P, Ambrogio C, Esteban-Burgos L, Gómez-López G, Blasco MT, Yao Z, Marais R, Rosen N, Chiarle R, Pisano DG, Barbacid M, Santamaría D. A Braf kinase-inactive mutant induces lung adenocarcinoma. *Nature* 2017; **548**:239–243.
90. Shojaee S, Caeser R, Buchner M, Park E, Swaminathan S, Hurtz C, Geng H, Chan LN, Klemm L, Hofmann WK, Qiu YH, Zhang N, *et al.* Erk negative feedback control enables pre-B cell transformation and represents a therapeutic target in acute lymphoblastic Leukemia. *Cancer Cell* 2015; **28**:114–128.
91. Marshall CJ. Specificity of receptor tyrosine kinase signaling: transient versus sustained extracellular signal-regulated kinase activation. *Cell* 1995; **80**:179–185.
92. Goriely A, Wilkie AO. Paternal age effect mutations and selfish spermatogonial selection: causes and consequences for human disease. *Am J Hum Genet* 2012; **90**:175–200.
93. Goriely A, Hansen RMS, Taylor IB, Olesen IA, Jacobsen GK, McGowan SJ, Pfeifer SP, McVean GAT, Meyts ERD, Wilkie AOM. Activating mutations in FGFR3 and HRAS reveal a shared genetic origin for congenital disorders and testicular tumors. *Nat Genet* 2009; **41**:1247–1252.
94. Georgescu MM, Islam MZ, Li Y, Traylor J, Nanda A. Novel targetable FGFR2 and FGFR3 alterations in glioblastoma associate with aggressive phenotype and distinct gene expression programs. *Acta Neuropathol Commun* 2021; **9**:69.